Elsevier Editorial System(tm) for Cement and Concrete Research
Manuscript Draft

Manuscript Number: CEMCON-D-14-00278R1

Title: The Role of the Alumina Content of Slag, plus the Presence of Additional Sulphate on the Hydration and Microstructure of Portland Cement-Slag Blends

Article Type: Research Paper

Keywords: Granulated Blast-Furnace Slag
; sulfate; hydration; microstructure; Characterization

Corresponding Author: Dr. Leon Black,

Corresponding Author's Institution: University of Leeds

First Author: Mark J Whittaker

Order of Authors: Mark J Whittaker; Maciej Zajac; Mohsen Ben Haha; Frank Bullerjahn; Leon Black

Abstract: The effects on composite cements of the aluminium content of slag plus that of additional sulphate, has been investigated. Samples containing cement or composites with 40% replacement by one of 2 different slags, differing in aluminium contents, were prepared. A further blended sample was prepared with additional anhydrite replacing 3%w/w of binder. Slag blended mortars showed comparable strengths to the neat cement system at later ages. Adding slag changed the hydration kinetics of the clinker phases. The addition of sulphate had no effect on slag reactivity but increased that of alite. Slags richer in aluminium resulted in greater incorporation of aluminium into C-S-H and encouraged the presence of hemicarbonate over monocarbonate. The Ca/Si ratios of the C-S-H formed were comparable between the two blends, being marginally lower than that of the neat system. The addition of anhydrite resulted in the adsorption of sulphate onto the C-S-H, plus stabilisation of ettringite.

The Role of the Alumina Content of Slag, plus the Presence of Additional Sulphate on the Hydration and Microstructure of Portland Cement-Slag Blends

Mark Whittaker[a], Maciej Zajac[b], Mohsen Ben Haha[b], Frank Bullerjahn[b], Leon Black[a,†]
[a]University of Leeds, Woodhouse Lane, Leeds, LS2 9JT
[b]Heidelberg Technology Center GmbH , Rohrbacher Str. 95, 69181 Leimen, Germany
[†]Corresponding Author

Abstract

The effects on composite cements of the aluminium content of slag plus that of additional sulphate, has been investigated. Samples containing cement or composites with 40% replacement by one of 2 different slags, differing in aluminium contents, were prepared. A further blended sample was prepared with additional anhydrite replacing 3%w/w of binder. Slag blended mortars showed comparable strengths to the neat cement system at later ages. Adding slag changed the hydration kinetics of the clinker phases. The addition of sulphate had no effect on slag reactivity but increased that of alite. Slags richer in aluminium resulted in greater incorporation of aluminium into C-S-H and encouraged the presence of hemicarbonate over monocarbonate. The Ca/Si ratios of the C-S-H formed were comparable between the two blends, being marginally lower than that of the neat system. The addition of anhydrite resulted in the adsorption of sulphate onto the C-S-H, plus stabilisation of ettringite.

1. Introduction

With a continual drive away from traditional cement systems, a better understanding of how the addition of supplementary cementitious materials (SCMs) affects hydration and the final phase assemblage is needed. Many current studies on composite systems focus on mechanical or durability aspects of specific SCMs but fail to inform the rest of community of the impact which the bulk composition, and the subsequent hydrates that are formed, have on the evolution of performance of composite cements[1].

Attempts have been made to determine reactivity and performance of blast furnace slags, based on chemical and mineralogical composition alone[2,3,4] and several hydraulic ratios have been summarised[2]. However, Mantel[5] tested various mixes and found no correlation between the more common ratios and performance. Despite this, there remains a strong dependence on such ratios, and they are incorporated into standards even; for example, it is required by BSI 197-1:2000 that $(CaO+MgO)/SiO_2$ should exceed 1[6].

Slags, whose slow hydration needs activation, produce analogous hydration products to cement, mainly a C-S-H, albeit with a lower Ca/Si ratio and increased Al/Si[7,8]. Furthermore, a change in aluminate, carbonate and sulphate content can further upset the hydrate assemblage, especially the ettringite and AFm distribution[9], while, a hydrotalcite-like phase may also form[1]. The quantity and composition of the hydrates formed are dependent on the composition of the starting materials that comprise the blend. Despite the slow hydration of the slag, leading to a lower degree of hydration at very early ages, slag blends can outperform neat cement systems at later ages with respect to strength[10,11]. The increased performance is dependent on both the phase assemblage and

microstructure. The hydration of slags in OPC blends can also be accompanied with some consumption of CH[12].

The present work focuses on the change in hydrate phase assemblages as cement is blended with blast furnace slag, and relates this to mechanical performance. Furthermore, the impact of the alumina content of the slag is also studied[13], as is the effect of sulphate level, an important additive to regulate setting time.

2. Materials and Methods

2.1. Materials

An industrial CEM I 42.5 R was chosen along with two ground granulated blast furnace slags of differing chemical compositions. The chemical compositions of each of these materials, as determined by XRF, are shown in Table 1, while **Figure 1** shows their respective particle size distributions. Tables 2 and 3 meanwhile give the mineralogical composition of the cement clinker and blast furnace slag respectively.

The slags have very comparable particle size distributions (**Figure 1**) and amorphous contents and vary primarily via their chemical composition. Considering the more abundant elements, slag C is richer in Ca, Al and Mg and slightly depleted in Si compared to slag B. The molar CaO/SiO_2 ratios for slags B and C are 0.96 and 1.12, respectively. The quartz used in the calorimetric study was almost pure SiO_2, containing approximately 1.7 % of impurities.

2.2. Methods

Pastes, with a w/b of 0.5, were cured in plastic vials and kept in a water bath at 20°C for 14 days before being transferred into a hydrated lime solution at 20°C. At predetermined time intervals, samples were characterised by XRD-Rietveld, thermogravimetric analysis (TG) and scanning electron microscopy (SEM).

The mix design of the different blends is shown in table 4. Additional pastes where the slag fraction was replaced with quartz of an equivalent particle size distribution were also prepared, so as to determine the filler effect.

Isothermal conduction calorimetry (ICC) was performed using a TAM Air twin-channel calorimeter. 6g of anhydrous binder was placed in a 20 mL plastic ampoule to which 3g of water (water/binder, w/b=0.5) was added. The pastes were shaken on a vortex mixer for 2 minutes at low speed. Measurements were taken over a period of 28 days, with quartz pastes as reference[14].

For quantitative XRD analysis, hydrated paste samples were crushed to a fine powder by manual grinding in a pestle and mortar without any prior hydration stopping, so as to minimise any damage to phases present[15,16]. The powders were backloaded into 16 mm diameter sample holders and diffraction patterns collected with a Philips Panalytical X'Pert MPD diffractometer equipped with a Cu Kα X-ray source, an X'Celerator detector and operated at 40kV and 40mA. Patterns were measured from 7 to 70^o 2θ with a step size of 0.0334^o. During collection, no carbonation of the sample was observed. Rietveld refinement of the patterns was conducted using the Philip's X'pert HighScore Plus programme version 2.2a (2.2.1). The XRD patterns were individually fitted for each sample, such to account for the amorphous phases (slag, C-S-H). The quantification of the X-ray amorphous phase content was conducted using the external standard method, using the G-factor method[17], with corundum (Al_2O_3) serving as the standard. Reference files were taken from the ICSD library.

The degree of slag hydration was measured by backscattered electron (BSE) image analysis[18]. 2mm thick disks were cut using a Struers Accutom-50 (Struers diamond cut-off wheel MOD 13) and freeze dried to constant weight. The samples were resin impregnated and then polished with silicon carbide paper followed by diamond paste. BSE images and elemental maps were obtained at a working distance of 8mm with an acceleration voltage of 15KeV. The degree of hydration was estimated on 50 images, collected at 800x. Note, the smallest features were not visible by this method, with a single pixel being 0.17x0.17 μm at 800x magnification. If we assume that the largest particles that cannot be captured are of the size of 2px*2px, then based on the particle size distribution shown in figure 1, at most 2 % of material is excluded[19].

For samples cured for 1, 28 and 180 days, EDS point analysis was also carried out on outer product (Op) and inner product (Ip) C-S-H, as well as the slag hydration rims when applicable. For Op C-S-H, 80 individual points were taken, whereas for Ip C-S-H and slag hydration rims 40 were collected. From plots of Si/Ca versus Al/Ca, Al/Si ratios were determined from the slope of the line originating from the origin drawn through the point with the lowest measured Al/Ca to best avoid intermixing with other phases[20]. The Ca/Si was taken as the point along that same line having the highest Si/Ca ratio. The Mg/Al for hydrotalcite-like phases in the blends was determined from the slope of a plot of Mg/Si versus Al/Si of the EDS data collected from slag hydration rims. The intersection of the slope with the abscissa gave the Al/Si of the C-S-H formed within the slag hydration rims.

The portlandite (CH) content and the amount of bound water W_n was measured on freeze-dried paste samples by thermal gravimetric analysis (TGA) analysis using a Stanton Redcroft 780 series under a nitrogen atmosphere, with a 20°C/min heating rate from 20 to 1000°C. Freeze drying was chosen over other drying methods, since it has been proposed as a suitable hydration stopping method for SEM and TGA analysis[15,21]. Zhang and Glasser[22] assessed that ettringite is susceptible to damage when vacuum drying, for example during freeze drying. This can potentially result in an underestimation of the bound water content, and a more gentle drying method would be advised for cementitious systems rich in ettringite. However ettringite is not a major phase in the systems presented here, and C_3A dilution in the blends further reduces its content. Therefore it is believed that the drying method should not affect the results strongly. The portlandite content was determined using the tangent method and the bound water was taken as the mass loss between 50°C and 550°C; with both sets of data normalised to the total mass loss at 550°C. The content measured by STA agreed with those measured by XRD, with a difference between the two sets of data being no greater than 1.5 %.

$$\%CH = \left(\frac{CH_w \times \left(\frac{M_{CH}}{M_{H_2O}} \right)}{W_{550}} \right) \times 100$$

where:
CH_w – mass loss of water bound to CH
M_{CH} – molar mass of CH, M_{CH}=74 g.mol^{-1}
M_{H_2O}– Molar mass of water, M_{H2O}=18 g.mol^{-1}

$$W_n = \left(\frac{W_{50} - W_{550}}{W_{550}} \right) \times 100$$

where:
W_{50}– mass loss at 50°C
W_{550} – mass loss at 550°C

Phase assemblage was modelled using GEMS (Gibbs Energy Minimisation)[23]. Thermodynamic data was taken from the PSI-GEMS database[24,25] along with cement specific data[26,27,28].

2.3. General overview of hydration

The bound water content gives an indication of the progress of hydration (figure 2a)[29,30] but cannot be directly related to the overall degree of hydration. All the blended systems showed a lower total bound water content, with C_140S_b showing the lowest. The addition of anhydrite in blend $C_140S_c\$$ had no noticeable impact upon the total bound water content. Similar results were found by Zajac. et. al. at longer hydration times for limestone composite cements[31].

The influence of binder composition could also be observed via development of the portlandite content (figure 2b). Replacement of cement clinker resulted in production of significantly lower levels of portlandite, since portlandite is produced only by the hydrating cement clinker. However, when normalised back to the cement content, the portlandite content in all slag blends was still lower than that of the neat system. Since slag hydration can be accompanied by portlandite consumption, to form C-S-H[12], the reduction in portlandite content was due to slag hydration[32]. There were also slight differences between the different slag blends. Slag B showed comparable levels of portlandite to C_1 for the first 7 days of hydration, after which there was a slight deviation as the portlandite content declined in the blend. However, for slag C the portlandite content was much lower from a very early stage, paired too with further, modest consumption as slag hydration progressed. This is possibly due to a change in composition of the slag, where slag C has a higher Ca/Si ratio. The addition of anhydrite in blend $C_140S_c\$$ encourages AFt formation requiring a source of calcium, more than that provided by anhydrite itself, and is sourced from CH. Hence its overall content is further reduced.

Blend composition did impact on compressive strength evolution (table 5). Replacement of the cement by 40% slag led to lower early-age strengths, but continued gradual strength development at later ages, such that all of the blends containing slag had comparable strengths to the neat system after 180 days; in line with previous research which has shown that slag cement blends can evolve equivalent or even greater strengths than neat cement systems at later ages[10,11,33]. Oner and Akyuz[11] estimated an optimum cement replacement level by slag of 55 % to reach a maximum strength. After 180 days of hydration, both the neat and the blended systems show comparable strength.

The preliminary results clearly show on-going hydration in all slag systems. This is seen firstly in the evolution of the bound water. The neat system C_1 showed little change in bound water beyond 7 days of hydration, by which time most of the clinker phases would have hydrated. However all the slag blends showed a continual increase. Furthermore, the portlandite content continually decreased over time in all the slag blends, most likely consumed by the slags. This indicates that hydration continued in the slag blend, such that all the investigated systems had comparable strengths after 180 days of hydration. A deeper investigation was therefore performed to better understand the interplay of hydration kinetics, phase assemblage and microstructure on the evolution of slag cement performance.

2.4. Hydration kinetics

Figure 3a shows the heat evolution rate for all blends, normalised to the cement content. The neat system was dominated by one peak, associated with alite hydration, followed by a very slight hump after 1 day, indicative of secondary aluminate reaction upon sulphate depletion[34,35,36]. The addition of slag was accompanied by an increase in the maximum heat rate of the alite phase; characteristic of the filler effect exacerbating clinker hydration. Furthermore, an additional peak was observed soon after the onset of the deceleration of alite hydration; this peak (labelled A) is analogous to the faint hump seen in the neat system C_1 and is due to the hydration of the aluminate phase under the

167 influence of the slag[1]. The occurrence of peak A was not constant in the slag blends; arising after
168 18h and 22.5 hours for $C_1 40S_c$ and $C_1 40S_b$ respectively. Since both slags had the same particle size
169 distributions, the known impact of particle fineness on the filler effect[37] can be discounted. Thus,
170 this difference was likely dependent on slag composition, with the aluminium-rich slag C showing a
171 slightly quicker reaction. The addition of anhydrite in $C_1 40S_c\$$ caused a delay in the hydration of the
172 aluminates[38], as previously demonstrated by Richardson *et. al*.[34].

173 Slag addition was accompanied by an increase in the total heat when normalised to the cement
174 content figure 3b. This effect was dependent on the slag type. The more basic, alumina-rich slag C
175 blend evolved more heat than the blend containing slag B. The addition of sulphates ($C_1 40S_c\$$) had
176 no effect on the total heat released, although early age hydration appeared to be accelerated. The
177 increase in reactivity per gram of clinker could be attributed to two distinct effects. Firstly, hydration
178 of the slag itself is exothermic[30,39]. Secondly, there is also the aforementioned filler effect[40,41], with
179 an increase in the water/cement ratio (table 4) plus the provision of nucleation sites, promoting
180 early-age clinker hydration[1]. This is illustrated in figure 3 where the blend $C_1 40Q$ contained 40%
181 quartz (which was assumed to be unreactive) in place of GGBS; any increased reactivity is therefore
182 attributed to the filler effect only.

183 ### 2.4.1. Hydration of the Cement Clinker

184 Hydration of the individual cement clinker phases was also followed by XRD (table 6). Alite
185 dissolution in the neat system was fast with over 90 % having reacted within 28 days in C_1; and 61 %
186 within just one day. Upon slag addition, alite hydrated more rapidly and only traces remained after
187 28 days. In contrast belite hydration was inhibited upon slag addition, but did eventually approach
188 the degree of hydration of the neat system.

189 C_3A was very reactive, with only traces being detected beyond 28 days of hydration in the neat
190 system C_1. Its reactivity was increased in the presence of slag with only traces remaining after just 2
191 days of hydration. The addition of sulphate however caused a delay in its reactivity but only
192 marginally; C_3A consumption was delayed compared to $C_1 40S_c$ but still faster than in the neat system
193 agreeing with the calorimetry observation.

194 Ferrite hydration was modest and only 59 % of the phase reacted within 28 days. Slag addition
195 accelerated ferrite hydration, such that after 28 days of hydration, 60 to 80 % had reacted in all
196 blended systems. The presence of additional sulphate had no discernable effect. This effect of slag
197 on the individual clinker phases is in agreement with the literature[42,43], and a similar effect has been
198 seen with ternary cement systems containing limestone powder and fly ash[44].

199 ### 2.4.2. Ground Granulated Blast-Furnace Slag

200 The degree of slag hydration was followed by BSE-IA, the results of which are plotted in figure 4.
201 After 1 day 20 % of slag in blend $C_1 40S_b$ had hydrated, while the figure for slag C was 26 %, whether
202 or not additional sulphate was added. After 1 year of hydration there was a clear difference in slag
203 reactivity between the mixes, with 57 % and 68 % of slag B (Al poor) and slag C (Al rich) having
204 reacted respectively. Slag reactivity is dependent on several factors; including w/b ratio and slag
205 fineness[45]. Because the slags' physical properties and the water/binder ratios in this study are
206 constant, this suggests that slag chemistry defines the degree of hydration provided that there is
207 sufficient activator, in this instance cement. The reactivity of slags has been previously investigated
208 based on their composition alone and several ratios have been proposed[2]. The most common is the
209 basicity ratio CaO/SiO_2 where good reactivity is expected for values greater than 1; Slag B and slag C
210 have a CaO/SiO_2 of 0.96 and 1.12 respectively.

The measured degrees of hydration agree with previous findings. Luke and Glasser[46] found that 41 % of the slag had reacted after 1 month of curing and 65% had reacted after a full year in blends containing 30 % slag. Similarly, Lumley et. al.[47] measured a degree of hydration varying from 30-55 % after 28 days of curing, and 45-75 % after 1 to 2 years of curing for blends with varying w/b and slag content. The difference measured here between slag B and slag C may very well be due to the change in composition and glass structure[2,48,49].

From figure 3, it was possible to separate the heat evolved from slag hydration from that of the clinker. The difference in heat evolution between the quartz blend, $C_1$40Q, and the neat system, C_1, is due solely to the filler effect. Therefore, the difference in heat evolution between a quartz- and slag-blend is due to the hydration of the slag itself, and this has been plotted in figure 5, normalised to the slag content. Slag C was more reactive than slag B, confirming SEM-BSE image analysis. At very early ages (less than 1 day), apparent zero values of heat released from the hydration of the slag was observed. This is likely to be the result of different interaction between the quartz, or slag, with the clinker; the very different composition between the quartz and slag would result in changes in the nature of the hydrates formed, most likely aluminates, and therefore resulting in minor changes in heat released at early stages. This suggests that the reactivity of slags remain low at very early ages confirming the SEM results. Slag C, the more reactive of the two slags, only reached a degree of hydration of 26 % after 1 day.

More interestingly, sulphate addition led to the appearance of an apparent maximum after 3-4 days. This was a consequence of a change in hydration kinetics of the aluminates in the presence of sulphates, as shown in figure 6. In blend $C_1$40S_c\$, peak A was observed after 2 days, whilst in the equivalent quartz blend ($C_1$40Q\$) the same peak appeared 5 days into the hydration. By comparison, in the blends not including additional sulphate ($C_1$40S_c and $C_1$40Q) peak A appeared after about 1 day of hydration. The difference in time explains the observed maximum following subtraction of the trace for $C_1$40Q. Because peak A is associated with aluminate hydration as sulphate is depleted, this would suggest an interaction between the sulphates and the slag allowing for a faster hydration of the sulphate and consumption of the aluminates[48,50,51].

This change in the kinetics of the aluminates in the presence of sulphates is confirmed in figure 7. In blends containing no added sulphate, C_3A hydration is fast, with only traces remaining in both blends $C_1$40Q and $C_1$40S_c. Upon sulphate addition, C_3A hydration is delayed however, more so in blend $C_1$40Q\$, where C_3A is present still after 7 days of hydration; confirming the calorimetric observations.

2.5. Hydration products

figure 8 shows typical BSE micrographs of the neat system C_1, compared to the blended system C140S_b. In the micrographs obtained from pastes cured for 2 days (figures 8a and 8b) there was an intimate mixture of anhydrous material, hydrated phases and pores. At this early stage a high proportion of anhydrous material was visible; ranging in size from just a few microns to 20µm or more. This was also true for the anhydrous slag particles. The more noticeable hydrates included calcium hydroxide (CH) appearing light grey, and outer product (Op) C-S-H, appearing dark grey. Since slags hydrate more slowly than Portland cement clinker, a higher porosity was noticeable at this early age in the blend compared to the neat system C_1. At later ages (figures 8 c and 8d), inner product C-S-H was more abundant, surrounding the partially hydrated larger grains. The finer slag particles had fully reacted leaving only partially hydrated larger ones with characteristic hydration rims. With increasing hydration the total pore area reduced.

2.5.1. C-S-H composition

The chemical composition of C-S-H was examined by SEM-EDX. The Ca/Si and Al/Si ratios of C_1 were shown to be constant over time, with a Ca/Si ≈ 1.8 and Al/Si ≈ 0.06 (table 7). Clinker replacement resulted in changes to C-S-H composition. In the case of slag B the Ca/Si ratio decreased to about 1.6 and remained approximately constant. The Al/Si ratio also remained constant, with a value close to 0.1. These values are similar to those in the literature; where the effect of slag on C-S-H composition and morphology are well reported and a C-S-H with a lower Ca/Si and higher Al/Si atomic ratio is ultimately formed[32,52,53,54].

The use of slag C induced greater changes in the C-S-H composition. Higher alumina contents in slag result in greater aluminium incorporation in the C-S-H. The Al/Si averaged 0.13 and again remained unchanged during hydration. The Ca/Si of the C-S-H was higher than for the equivalent blend made with slag B, due to the higher CaO/SiO_2 of the slag.

The addition of extra sulphate resulted in a slight increase in the Ca/Si ratio with the Al/Si atomic ratios of the C-S-H at later ages similar to the blends without additional sulphate. However, the addition of sulphate did lower the Al/Si ratio at 1 day. At this early stage, there was still some residual anhydrite in the paste and so ettringite was preferentially precipitated over the AFm phases. The aluminium concentration in solution was thus defined by the low solubility of ettringite[55], therefore aluminium incorporation into the C-S-H remained low. Additionally the S/Ca atomic ratio increased (table 7) in $C_140S_c\$$, in line with similar, previous studies[56,57,58,59]. The coupled increase of both Ca and S content in the C-S-H suggests the absorption of calcium sulphate on C-S-H, as predicted by Labbez et al.[60].

2.5.2. Effect of Slag composition and Added Sulphate

The ettringite contents, as determined by XRD-Rietveld, are summarised in figure 10. All hydrating systems quickly reached a stable plateau within the first few days of hydration. In the neat system, C_1, 17g of ettringite was produced from 100g of cement. Slag addition reduced the ettringite content, with both slags behaving similarly. Therefore, the lower sulphate content of these blends dominated over the increased aluminium content (table 1). The addition of sulphate in blend $C_140S_c\$$ led to an increase in ettringite content, exceeding those of C_1. There was no indication of the conversion of ettringite to AFm, with the former stabilised by the addition of limestone in the clinker[44,61,62].

The addition of slag to blends altered the chemistry of the hydration products; and figure 11 shows the evolution of the AFt and AFm phases in all the systems, as measured by XRD. Throughout the study ettringite was present in the neat system, but crystalline AFm was absent. As hydration proceeded, hemicarbonate (Hc) was formed beyond 7 days and progressively transformed to monocarbonate (Mc), agreeing with previous studies[59,62,63]. Upon the addition of slag, provision of aluminium led to formation of hemicarbonate within one day. In the case of C_140S_b, the subsequent progressive conversion of Hc to Mc started after 7 days of hydration and was almost complete after a year. In the more Al-rich C_140S_c, Hc persisted and its conversion to Mc was only partial. The addition of sulphates in blend $C_140S_c\$$ further upset the AFt-carboaluminate distribution. The reflections for ettringite were more intense, but at the expense of the carboaluminate phases. Just like its sulphate free equivalent, after 7 days of hydration, there was a strong Hc reflection, but this was converted to Mc as hydration progressed. In the neat blends, the overall peak shapes of the AFm phases were mostly well defined making their identification easy. The overall shapes of the phase were more obtuse in the slag blends, however. As such, care should be taken when assigning

reflections to the AFm phases, as their low crystallinity and variability in composition can result in peak shift and changes in intensity[9,62]. Hydrotalcite (Ht) was present in all systems, the amount of which was greatest in the blended systems due to the higher magnesium content of the slags.

The effect of slag on the AFm phase distribution is further highlighted in figure 12, showing blends where the slag fraction has been replaced with quartz. In blend $C_1$40Q, ettringite was present after just 1 day of hydration and Hc precipitated after 2 days. Compared to its slag-containing cousin, Hc was present after just 1 day with much stronger peak intensities. C_3A hydration (figure 7) was comparable between blends $C_1$40Q and $C_1$40Sc suggesting that the slag acts as an Al_2O_3 reservoir promoting earlier Hc precipitation in the slag blend. When adding sulphates, in blend $C_1$40Q$, ettringite continuously precipitated, highlighting the slower dissolution of C_3A, and Hc was never present. In comparison to the sulphated slag blend, ettringite showed the strongest peak intensities and was present in full by 2 days (figure 10), and Hc was present in minor quantities after just 2 days of hydration. C_3A hydration was delayed in blend $C_1$40Q$ (figure 7); where there was too little alumina to compensate for the additional sulphate, thus preventing any AFm precipitation within 7 days of hydration. This confirms the role of slag alumina content on the hydrates formed.

These results can be explained by the findings of Matschei et al[9]. The hydration of C_3A with sulphates produces ettringite and sulphate-AFm phases. In the blend quartz blend spikes with sulphate, the SO_3/Al_2O_3 is sufficiently high enough for only ettringite to precipitate. With the slag blend, more aluminium is available, effectively reducing the overall SO_3/Al_2O_3 allowing more AFm to precipitate at the expense of ettringite. With calcite in the system, added to the clinker, carbonate AFm phases are predicted to over sulphate AFm, as they are more stable in the presence of calcite.

2.6. Slag Hydration Rims

Slag hydration is associated with the formation of a hydrotalcite-like phase. Unlike pure hydrotalcite, where the Mg/Al is equal to 3, a ratio closer to 2 is more common in slag cement blends[64]. Mg/Al ratios were obtained from the slope of the line of best fit when plotting Mg/Si against Al/Si (figure 13). Data were obtained from slag hydration rims on samples cured for 180 days, where the rims were sufficiently large enough to be measured with minimal interference from the surrounding hydrates. The Mg/Al of the slag rims was highest in blend $C_1$40S_b, at 2.67. Replacement of slag B with slag C led to a slight reduction in the Mg/Al ratio of the hydrotalcite, to 2.01. XRD patterns showed only slight traces of hydrotalcite in the neat system C_1 (figure 11). However it was not possible to observe hydrotalcite by SEM, it being finely intermixed with the C-S-H, and therefore no EDX analysis could be performed.

This reduction in Mg/Al for the blend containing slag C was likely due to differences in slag composition. Slag C contained more aluminium and magnesium than slag B, but had a lower bulk Mg/Al ratio (0.89 versus 1.19). The increased aluminium content may explain the higher levels of calcium hemicarbonate hydrate and the increased aluminium incorporation into the Op C-S-H. However, with magnesium remaining immobile[65] and not being incorporated into C-S-H but rather finely intermixed[66], the lower initial bulk Mg/Al led to a lower Mg/Al ratio in the hydrotalcite. This observation is in line with those of Ben Haha et. al. who measured a much lower Mg/Al for the hydrotalcite like phase when the bulk Mg/Al of the anhydrous slag was much lower[67]. Furthermore as the MgO content increases in a blend, more hydrotalcite is expected to form requiring a greater amount of Al, but also potentially reducing porosity and improving strength[68]. Although poorly resolved in XRD patterns[69], there appears to be a greater, albeit broad, hydrotalcite reflection indicating a greater amount of hydrotalcite in blends using slag C.

However when extra sulphates were added, there was a marked increase in the hydrotalcite Mg/Al ratio, due to aluminium being incorporated in hydrate phases elsewhere. The addition of calcium sulphate resulted in a lower Al/Si of the Op C-S-H at early ages only to increase as hydration proceeded. The additional anhydrite was accompanied by a reduction in portlandite which was consumed with the anhydrite to stabilise ettringite over monosulphate (figure 11). As a result, less alumina was available in solution for the formation of the hydrotalcite phase, resulting in the observed increase in the Mg/Al.

Figure 13 also allows the Al/Si ratio of the C-S-H within the slag hydration rims, estimated assuming hydrotalcite to be free from Si. The values are slightly higher than those measured for the Op C-S-H of the blended systems since the slags are richer than the clinker in aluminium.

2.7. Discussion

SEM-BSE analysis also enabled determination of the capillary porosity. Figure 14 shows a clear negative correlation between porosity and compressive strength. Only the coarser porosity was evaluated using this approach, as the finer porosity was invisible to the SEM. This suggests that the coarse porosity dominates the compressive strength, independent of the mix designs, which is in agreement with previous observations[44, 70,71,72].

At later ages (180 days) the samples are characterized by a similar low coarse porosity and high compressive strength. However, data from figures 3 and 4, plus table 6, show that the degree of hydration was lower in the slag blends. This is confirmed by thermodynamic modelling (figure 15), which showed clinker replacement with slag to reduce the total volume of hydrates. It was assumed that the cement had reached 100% degree of hydration and that slag, using the composition of slag C, had reached a degree of hydration 70 %. This corresponds to the situation after roughly 360 days of hydration. The C-S-H phase was modelled having a Ca/Si of 1.6 and an Al/Si of 0.1 (table 7). However, as shown above, the capillary porosity, and therefore the strength, doesn't change. This implies that the capacity of the hydrates to fill the pore space in the OPC and slag blended cement is different. It is known that the properties of the C-S-H phase are modified in the presence of slag, for example the microstructure[52,53] and this may be responsible for that phenomenon.

Figure 16 illustrates the effect of changing the Al_2O_3 content in the slag on the phase assemblage. The models assumed the same composition of the C-S-H plus the same degree of hydration as in figure 15. The differences in phase assemblage here only reflect the changes in composition of the slag, ignoring any kinetic effect of the 2 slags. Increasing the Al_2O_3 content of the slag from that of Slag B (7.4 % Al_2O_3) to that of slag C (12.3 % Al_2O_3) leads to the formation of AFm phases (Mc and Hc) while decreasing the total volume of the C-S-H phase, slightly increasing the total hydrate volume. With such a slight increase in volume, it is unlikely that the increasing the Al_2O_3 content would greatly affect the strength. As such the differences in strength (table 5) between blends using slag B and C are due to the hydration kinetics of the slags (figure 4).

Additionally, modelling results agree very well with the changes in the phase assemblage shown in figures 10 and 11 The limestone within the cement ensured that the ettringite content remained constant and that the formation of the carboaluminates became increasingly prominent. Modelling reveals that the calcium demand for the formation of the additional AFm phases is rather limited. The model also predicted that increasing the Al_2O_3 content in the slag from 7 % to 12 % reduced the portlandite content. The modelled reduction in portlandite was experimentally observed in figure 2, when substituting slag B with slag C. This suggests that the changes between samples C_140S_b and C_140S_c are related to changes in the C-S-H (table 7).

Although C-S-H is the primary hydrate responsible for strength, the amount and type of aluminate hydrates formed also play a role in space filling[73]. It is important to note the effects associated with changes in AFm phases and ettringite. The stabilisation of ettringite with addition of extra sulphate leads to an increase in the volume of hydration products (figure 17), and thus one would expect an increase in compressive strength. Nevertheless, comparing blends $C_1 40 S_c$ and $C_1 40 S_c \$$, the latter has a slightly higher porosity, and lower compressive strength at later ages, despite a similar degree of hydration. This is true despite the lower density of ettringite which is much more prevalent in $C_1 40 S_c \$$ (figure 10 and figure 16). Studies[74,75] have shown that the addition of a small quantity of sulphates enhanced strength; but higher levels led to a decrease in strength. Gunay et. al[76] showed that the nucleation growth process of the C-S-H is modified as calcium sulphate is adsorbed on the C-S-H. The lower strength found here could be due to a reduced particle force between C-S-H as measured by Medala[77]. Sersale et. al.[78] found that the mechanical resistance and amount of porosity varied with sulphate content. This study suggests that the sulphate can have a negative impact on the filling capacity of the C-S-H as already shown in the literature[31].

3. Conclusions

Despite slower hydration kinetics of slag, and therefore a lower degree of hydration of composite cements, the performance of slag cements can surpass that of neat cements at later ages. This is because of changes in composition and phase assemblage which ultimately depends on the starting bulk composition; where slags have much higher alumina and magnesia contents, and lower calcium and silica contents than cement. Furthermore, the sulphate content can further alter the phase assemblage.

The overall hydration of the clinker seemed unaffected by the presence of slag, with over 50 % of the clinker having reacted after just 1 day. The hydration kinetics of the individual clinker phases were affected, with C_3S, C_3A and C_4AF being accelerated, and C_2S retarded. But, there was no discernible influence of the slag composition. However, the extent of slag hydration increased with Ca/Si and Al_2O_3 content in the investigated range. The addition of anhydrite to a slag blend exacerbated the hydration of alite, but did not affect the kinetics of slag hydration

Slag addition affected C-S-H composition, with a reduction in Ca/Si and an increase in Al/Si. The extent of these changes was dependent upon slag composition, with the more basic slag B (C/S = 0.96) yielding C-S-H with a lower Ca/Si than slag C (C/S = 1.12). Sulphates further affected the composition such that the apparent Ca/Si of the C-S-H increased as calcium sulphates were adsorbed on its surface. At later ages the Al/Si of the C-S-H was not affected by sulphate addition, but was much lower at early ages since it was controlled by the low solubility of ettringite.

Changing the starting composition of a blend also affected the AFm phase distribution, chiefly with the increased alumina available in a blend; which is reflected in the AFm phases formed and the amount of ettringite present. Slag C, richest in alumina, favoured the formation of calcium hemicarboaluminate, even at later stages of hydration. The composition of the slag also had an effect on the hydrotalcite-like phase seen in all blended systems; with the Mg/Al ratio varying with the same ratio in the slag. More interestingly, the addition of extra sulphates resulted in an increase in the hydrotalcite Mg/Al ratio as more alumina was consumed to form ettringite.

Changes in modelled phase assemblages have shown a decrease in paste volume with an increase in slag content. At a given level of replacement, e.g. 40 %, the total phase volume increased with the sulphate content, where the overall ettringite content continually increased. Increase in the

alumina content in the slag, for a given hydration degree increased the total volume of hydrates only slightly.

The results demonstrate that slags have two main effects on performance; firstly, their hydration increased the hydrate volume, secondly they modify the phase assemblage, changing the capacity for pore space filling. Both processes result in an increase in the compressive strength. However, the addition of sulphate had only positive impact on the early age strength.

4. Acknowledgements

This work was funded by a University Research Scholarship from the University of Leeds for MJW, with additional funding and materials provided by HeidelbergCement Technology Centre GmbH.

List of Tables

List of Figures

479

480 **Table 1 - Compositions of Raw Material, Determined by XRF (% Weight)**

		CEM1	Slag B	Slag C
LOI 950 °C	%	2.62	(+0.85)*	(+1.57)*
SiO_2	%	19.21	39.75	34.35
Al_2O_3	%	5.50	7.36	12.33
TiO2	%	0.27	0.25	0.93
MnO	%	0.04	2.54	0.4
Fe_2O_3	%	2.77	1.33	0.52
CaO	%	62.28	38.18	38.49
MgO	%	2.19	7.65	9.58
K_2O	%	0.93	0.65	0.48
Na_2O	%	0.08	0.13	0.24
SO_3	%	3.10	1.83	2.61
P_2O_5	%	0.17	0.01	0.01
Total	%	99.15	99.69	99.93

*The sample was oxidized with HNO_3 before determination of LOI

481 **Table 2 - Clinker Content of C_1 (%Weight)**

Phases	C_1
C_3S M3 [%]	61
β-C_2S [%]	11.9
C_3A [%]	7.5
C_4AF [%]	8.3
Calcite [%]	3.7
anhydrite [%]	2.9
Hemihydrate [%]	1.5
other [%]	3.2

482

483

484 **Table 3 - Phases Present and Amorphous Content of the Slags (% Weight)**

Phases	Slag B	Slag C
Calcite [%]	0.4	0.7
Quartz [%]	0.2	0.0
Gehlenite [%]	0.4	1.0
Amorphous content [%]	99.0	98.3

485

486 **Table 4 - Mix Design of all Blends**

	C_1	C_140S_b	C_140S_c	$C_140S_c$$
CEM I	1.00	0.60	0.60	0.58
slag	-	0.40	0.40	0.39
anhydrite	-	-	-	0.03
w/binder	0.50	0.50	0.50	0.50
w/cement	0.50	0.83	0.83	0.86

487

488

489

Table 5 – Unconfined Compressive Strength (MPa)

Time	C_1		C_140S_b		C_140S_c		C_140S_c\$	
Days	MPa	σ	MPa	σ	MPa	σ	MPa	σ
1	13.0	0.5	7.1	0.2	7.2	0.2	5.9	0.3
2	27.0	0.7	13.6	0.5	16.6	0.2	16.6	0.3
7	46.2	1.5	32.5	0.9	35.4	1.2	36.8	0.6
14	49.9	1.7	43.9	1.4	45.3	2.5	42.0	1.9
28	52.5	2.0	45.4	1.1	49.3	0.6	48.1	1.1
180	55.6	2.7	53.6	2.6	56.3	3.0	52.9	2.7

490

491

Table 6- Evolution of Clinker Phases with Hydration (/100g of binder, error=±2%)

	time [d]	C_3S	C_2S	C_3A	C_4AF	CH (TGA)	AFt	DoH OPC
C1	**0**	61.0	11.9	7.5	8.3	0.7	0.0	0
	1	23.6	11.0	4.1	6.8	10.8	17.2	49
	7	4.6	9.7	0.9	3.8	16.9	17.2	79
	14	5.8	9.0	0.9	3.6	16.7	16.5	78
	28	5.2	8.8	0.5	3.4	17.7	16.4	80
	180	2.2	4.3	-	3.6	18.0	16.5	88
	360	0.1	3.6	-	3.8	18.2	16.6	92
C140Sb	**0**	36.8	6.4	4.5	4.5	0.4	0.0	0
	1	15.2	6.7	1.2	3.2	7.1	9.9	49
	7	0.3	6.6	-	1.4	10.2	10.5	83
	14	0.7	6.5	-	1.4	9.9	9.9	83
	28	1.1	6.3	-	1.3	9.7	10.2	83
	180	1.0	2.6	-	1.1	8.5	9.7	91
	360	0.9	1.7	-	1.2	8.8	10.1	93
C140Sc	**0**	37.8	6.0	4.3	4.8	0.5	0.0	0
	1	16.4	6.2	1.3	3.6	5.5	9.7	48
	7	3.3	6.1	-	2.0	7.9	9.4	78
	14	2.0	6.1	-	2.2	7.9	8.9	80
	28	1.2	6.0	-	1.4	8.4	9.4	83
	180	1.9	2.7	-	0.9	7.4	8.9	89
	360	0.4	1.7	-	0.8	6.6	8.6	95
C140Sc\$	**0**	36.4	5.8	4.0	4.3	0.4	0.0	0
	1	12.1	5.9	2.5	3.2	4.5	15.0	53
	7	2.6	5.7	-	1.8	6.5	17.8	79
	14	3.7	6.2	-	1.9	6.2	18.6	76
	28	3.1	6.0	-	1.8	6.4	18.2	78
	180	0.9	3.4	-	1.3	5.9	18.1	89
	360	2.2	1.4	-	1.4	5.3	18.0	89

492

493

494

495

496

497

498 Table 7 - Various Atomic Ratios of the Op C-S-H Phase (error= ±0.005)

	days	C_1	C_140S_b	C_140S_c	$C_140S_c$$
Ca/Si	1	1.85	1.61	1.67	1.78
	28	1.82	1.56	1.65	1.75
	180	1.81	1.59	1.72	1.72
Al/Si	1D	0.06	0.12	0.14	0.08
	28D	0.07	0.11	0.12	0.13
	180D	0.06	0.09	0.12	0.12
S/Ca	1D	0.07	0.05	0.05	0.09
	28D	0.05	0.04	0.04	0.05
	180D	0.04	0.01	0.02	0.04

499

500 Complementary text for Figure 13

	C140Sb	C140Sc	C140Sc$
Al/Si	0.1	0.13	0.15
Mg/Al	2.67	2.01	2.2

501

502

503

[1] LOTHENBACH, B., SCRIVENER, K., HOOTON, R.D., Supplementary Cementitious Materials, Cement and Concrete Research, 41, 2011, pp. 1244-1256

[2] SMOLCZYK, H.G., Slag Structure and Identification of Slags, Proceedings of the 7th International Congress on the Chemistry of Cement, Paris, France, I, III 1/3-1/17, 1980

[3] PAL, S.C., MUKHERJEE, A., PATHAK, S.R., Investigation of Hydraulic Activity of Ground Granulated Blast Furnace Slag in Concrete, Cement and Concrete Research, 33, pp. 1481-1486, 2003

[4] WANG, P.Z., TRETTING, R., RUDERT, V., SPANIOL, T., Influence of Al_2O_3 Content on Hydraulic Reactivity of Granulated Blast-Furnace Slag, and the Interaction Between Al_2O_3 and CaO, Advances in Cement Research, 2004, 16, 2004, pp. 1-7

[5] MANTEL. D.G., Investigation into the Hydraulic Activity of Five Granulated Blast Furnace Slags with Eight Different Portland Cements, ACI Materials Journal, 91(5), pp. 471-477, 1994

[6] BRITISH STANDARD INSTITUTION, BS EN 197-1:2000, Cement-Part 1: Composition, Specification and Conformity Criteria for Common Cements, BSI 2000

[7] DUSCHESNE, J., BERUBE, M.A., Effect of Supplementary Cementing Materials on the Composition of Cement Hydration Products, Advanced Cement Based Materials, 2 (2), 1995, pp 43-52

[8] RICHARDSON, I.G., GROVES, G.W., The Incorporation of Minor and Trace Elements into Calcium Silicate Hydrates (C-S-H) Gel in Hardened Cement Pastes, Cement and Concrete Research, 23, 1993, pp131-138

[9] MATSCHEI, T., LOTHENBACH, B., GLASSER, F.P., The AFm Phase in Portland Cement, Cement and Concrete Research, 37, 2007, pp. 118-130

[10] BOUGARA, A., LYNSDALE, C., MILESTONE, N.B., Reactivity and Performance of Blast furnace Slags of Different Origin, Cement and Concrete Composites, 32, 2010, pp. 319-324

[11] ONER, A., AKYUZ, S., An Experimental Study on Optimum Usage of GGBS for the Compressive Stength of Concrete, Cement and Concrete Composite, 29, 2007, pp. 505-514

[12] KOLANI, B., BUFFO-LACARRIERE, L., SELLIER, A., ESCADEILLAS, G., BOUTILLON, C., LINGER, L., Hydration of Slag-Blended Cements, Cement and Concrete Composites, 34, 2012, pp. 1009-1018

[13] WASSING, W., Improving the Early Strength of Blast furnace Cement Mortars and Concretes by Fixation of Silicate Hydrogels with Reactive Aluminates, Cement International, 5, 2008, pp. 63-79

[14] WADSO, L., Operational Issues in Isothermal Calorimetry, Cement and Concrete Research, 40, 2010, pp. 1129-1137

[15] COLLIER, N.C., SHARP, J.H., MILESTONE, HILL, J., GODFREY, I.H., The Influence of Water Removal Techniques on the Composition and Microstructure of Hardened Cement Pastes, Cement and Concrete Research, 38, 2008, pp. 737-744

[16] ZHANG, J., SCHERER, G.W., Comparison of Methods for Arresting Hydration of Cement, Cement and Concrete Research, 41, 2011, pp. 1024-1036

[17] JANSEN, D., GOETZ-NEUNHOEFFER, F., STABLER, C., NEUBAUER, J., A Remastered External Standard Method Applied to the Quantification of Early OPC hydration, Cement and Concrete Research, 41, 2011, pp. 602-608

[18] KOCABA, V., GALLUCCI, E., SCRIVENER, K.L., Methods for Determination of Degree of Hydration of Slags in Blended Cement Pastes, Cement and Concrete Research, 2012, pp. 511-525

[19] BEN HAHA, M., DE WEERDT, K., LOTHENBACH, B., Quantification of the Degree of Reaction of Fly Ash, Cement and Concrete Research, 40, 2010, pp. 1620-1629

[20] DESCHNER, F., WINNEFELD, F., LOTHENBACH, B., SEUFERT, S., SCHWESIG, P., DITTRICH, S., GOERZ-NEUNHOEFFER, F., NEUBAUER, J., Hydration of Portland Cement with High Replacement by Siliceous Fly Ash, Cement and Concrete Research, 42, 2012, pp. 1389-1400

[21] ZHANG, J., SCHERER, G.W., Comparison of Methods for Arresting Hydration, Cement and Concrete Research, 41, 2011, pp. 1024-1036

[22] ZHANG, L., GLASSER, F.P., Critical Examination of Drying Damage to Cement Pastes, Advances in Cement Research, 2000, 12 (2), pp.79-88

[23] KULIK, D., GEMS 2, software, http://gems.web.psi.ch/ PSI, Villigen, Switzerland, 2010

[24] THOENEN, T., KULIK, D., Nagra/PSI chemical thermodynamic database 01/01 for GEMS-selektor (V.2-PSI) geochemical modelling code, http://gems.web.psi.c/doc/pdf/TM-44-03-04-web.pdf PSI, Villigen, 2003

[25] HUMMEL, W., BERNER, U.,CURTI, E., PEARSON, F.J., THOENEN, T., Nagra/PSI chemical thermodynamic data base 01/01, Universal Publishers/uPUBLISH.com, USA also published as Nagra Technical Report NTB 02-16, Wettingen, Switzerland 2002, 2002.

[26] LOTHENBACH, B., WINNEFELD, F., Thermodynamic modelling of the hydration of Portland cement, Cement and Concrete Research, 36, 2006, pp. 209–226

[27] MATSCHEI, T., LOTENBACH, B., GLASSER, F.P., Thermodynamic properties of Portland cement hydrates in the system CaO–Al2O3–SiO2–CaSO4–CaCO3–H2O, Cement and Concrete Research, 37, 2007, pp. 1379–1410

[28] LOTHENBACH, B., MATSCHEI, T., MOSCHNER, G., GLASSER, F.P., Thermodynamic modelling of the effect of temperature on the hydration and porosity of Portland cement, Cement and Concrete Research, 38, 2008, pp. 1–18

[29] MARSH, B.K., DAY, R.L, Pozzolanic and cementitious reactions of fly ash in blended cement pastes, Cement and Concrete Research, 18, 1988, pp. 301-310.

[30] PANE, I., HANSEN, W., Investigation of blended cement hydration by isothermal calorimetry and thermal analysis, Cement and Concrete Research, 35, 2005, pp. 1155-1164.

[31] ZAJAC, M., ROSSBERG, A., LE SAOUT, G., LOTHENBACH, B., Influence of limestone and anhydrite on the hydration Portland cements, Cement and Concrete Composites, 46, 2014, pp. 99-108.

[32] TAYLOR, R., RICHARDSON, I.G., BRYDSON, R.M.D., Composition and microstructure of 20-year-old ordinary Portland Cement-Ground Granulated Blast-furnace Slag Blends Containing 0-100 % Slag, Cement and Concrete Research, 40, 2010, pp. 971-983

[33] BARNETT, S.J., SOUTSOS, M.N., MILLARDS, S.G., BUNGEY, J.H., Strength Development of Mortars Containing Ground Granulated Blast-Furnace Slag: Effect of Curing Temperature and Determination of Apparent Activation Energies, Cement and Concrete Research, 36, 2006, pp. 434-440

[34] RICHARDON, I.G., WILDING, C.R., DICKSON, M.J., The Hydration of Blast furnace Slag Cements, Advances in Cement Research, 2(8), 1989, pp. 147-157

[35] LERCH, The Influence of Gypsum on the Hydration and Properties of Portland Cement Pastes – Discussion, Proc. American Society for Testing Materials, 46, 1946, pp. 1252-1297

[36] HESSE, C., GOETZ-NEUNHOEFFER, F., NEUBAUER, J., A New Approach in Quantitative in-situ XRD of Cement Pastes: Correlation of Heat Flow Curves with Early Hydration Reactions, Cement and Concrete Research, 41, 2011, pp. 123-128

[37] LAWRENCE, P., CYR, M., RINGOT, E., Mineral Admixtures in Mortars – Effect of Inert Materials on Short Term Hydration, Cement and Concrete Research, 33, 2003, pp. 853-861

[38] MINARD, H., GARRAULT, S., REGNAUD, L., NONAT, A., Mechanisms and Parameters Controlling the Tricalcium Aluminate Reactivity in the Presence of Gypsum, Cement and Concrete Research, 37, 2007, pp. 1418-1426

[39] SHI, C., DAY, R.L., A Calorimetric Study of Early Hydration of Alkali-Slag Cements, Cement and Concrete Research, 25, 1995, pp1333-1346

[40] GUTTERIDGE, A. W., DALZIEL, J. A., Filler Cement: The Effect of the Secondary Component on the Hydration of Portland Cement Part 1 – A Fine Non-Hydraulic Filler, Cement and Concrete Research, 20, 1990, pp. 778-782

[41] GUTTERIDGE, A. W., DALZIEL, J. A., Filler Cement: The Effect of the Secondary Component on the Hydration of Portland Cement Part 2 – Fine Hydraulic Binders, Cement and Concrete Research, 20, 1990, pp. 853-861

[42] KOCABA, V., Development and Evaluation of Methods to Follow Microstructural Development of Cementitious Systems Including Slags, Phd Thesis, EPFL, 2009

[43] SCRIVENER, K.L., NONAT, A., Hydration of Cementitious Materials, Present and Future, Cement and Concrete Research, 41, 2011, pp. 651-665

[44] DE WEERDT, K., BEN HAHA, M., LE SAOUT, G., KJELLSEN, K.O., JUSTNES, H., LOTHENBACH, B., Hydration Mechanisms of Ternary Portland Cements Containing Limestone Powder and Fly Ash, Cement and Concrete Research, 41, 2011, pp. 279-291

[45] ESACALANTE-GARCIA, J.I., GOMEZ, L.Y., JOHAL, K.K., MENDOZA, G., MANCHA, H., MENDEZ, J., Reactivity of Blast-Furnace Slag in Portland Cement Blends Hydrated Under Different Conditions, Cement and Concrete Research, 31, 2001, pp. 1403-1409

[46] LUKE, K., GLASSER, F.P., Selective Dissolution of Hydrated Blast Furnace Slag Cements, Cement and Concrete Research, 17, 1987, pp. 273-282

[47] LUMLEY, J.S., GOLLOP, R.S., MOIR, G.K., TAYLOR, H.F.W., Degrees of Reaction of the Slag in Some Blends with Portland Cements, Cement and Concrete Research, 26, 1995, pp. 139-151

[48] REGOURD, M., Structure and Behaviour of Slag Portland Cement Hydrates, Proceedings of the 7th International Congress on the Chemistry of Cement, Paris, France, I, III 2/10-12/26, 1980

[49] UCHIKAWA, H., UCHIDA, S., Effect of Character of Glass Phase in Blending Components on their Reactivity in Calcium Hydroxide Mixture, 8th International Congress on the Chemistry of Cement, Rio de Janeiro, vol 4., pp. 245-250, 1986

[50] MATSCHEI, T., BELLMAN, F., STARK, J., Hydration Behaviour of Sulphate-Activated Slag Cements, Advances in Cement Research, 17(4), 2005, pp. 167-178

[51] DUTTA, D.K., BORTHAKUR, P.C., Activation of Low Lime High Alumina Granulated Blast Furnace Slag by Anhydrite, Cement and Concrete Research, 20, 1990, pp. 711-722

[52] RICHARDSON, I.G., GROVES, G.W., Microstructure and Microanalysis of Hardened Cement Pastes Involving Ground Granulated Blast-Furnace Slag, Journal of Materials Science, 27, 1992, pp 6204-6212

[53] RICHARDSON, I.G., GROVES, G.W., The structure of the calcium silicate hydrate phases present in hardened pastes of white Portland cement blast-furnace slag blends, Journal of Materials Science, 32(18), 1997, pp. 4793–4802.

[54] RICHARDSON, I.G., The nature of C–S–H in hardened cements, Cement and Concrete Research, 29, 1999, 1131–1147.

[55] LOTHENBACH, B., Thermodynamic Equilibrium Calculations in Cementitious Systems, Materials and Structures, 43, 2010, pp. 1413-1433

[56] COPELAND, L.E., KANTRO, D.L., Hydration of Portland cement, 5th International Congress on the Chemistry of Cement, Tokyo, 1968, Vol. 2, pp.387-420

[57] BENTUR, A., Effect of gypsum on the hydration and strength of C3S pastes, Journal of the American Ceramic Society, 59(5-6), 1976, pp. 210-213

[58] BARBARULO, R., PEYCELON, H., LECLERCQ, S., Chemical equilibria between C–S–H and ettringite, at 20 and 85 °C, Cement and Concrete Research, 37, 2007, pp. 1176-1181.

[59] ZAJAC, M., ROSSBERG, A., LE SAOUT, G., LOTHENBACH, B., Influence of limestone and anhydrite on the hydration Portland cements, Cement and Concrete Composites, 46, 2014, pp. 99-108.

[60] LABBEZ, C., POCHARD, I., NONAT, A., JONSSON, B., Colloidal behavior of C-S-H nanohydrates in cement paste, Proceedings of the CONMOD 2010, Lausanne, Switzerland, 2010

[61] KUZEL, H.J., POLLMAN, H., Hydration of C3A in the Presence of Ca(OH)2, CaSO4.2H2O and CaCO3, Cement and Concrete Research, 21, 1991, pp. 885-895

[62] LOTHENBACH, B., LE SAOUT, G., GALLUCCI, E., SCRIVENER, K., Influence of Limestone on the Hydration of Portland Cements, Cement and Concrete Research, 38, 2008, pp. 848-860

[63] KALALI, G., TSIVILIS, S., AGGELI, E., BATI, M., Hydration products of C3A, C3S and Portland cement in the presence of CaCO3, Cement and Concrete Research, 30, 2000, pp. 1073-1077

[64] WANG, S.D., SCRIVENER, K.L., Hydration Products of Alkali Activated Sag Cement, Cement and Concrete Research, 25, 1994, pp. 561-571

[65] HEWLETT, P.C., Lea's Chemistry of Cement and Concrete, Oxford, Butterworth-Heinemann, 1998

[66] RICHARDSON, J.M., BIERNACKI, J.J., STUTZMAN, P.E., BENTZ, D.P, Stoichiometry of Slag Hydration with Calcium Hydroxide, Journal of the American Ceramic Society, 85, 2002, pp. 947-953

[67] BEN HAHA, M., LOTHENBACH, B., LE SAOUT, G., WINNEFELD, F., Influence of Slag Chemistry on the hydration of Alkali-Activate Slag – part 2: Effect of Al_2O_3, Cement and Concrete Research, 42, 2012, pp. 74-83

[68] BEN HAHA, M., LOTHENBACH, B., LE SAOUT, G., WINNEFELD, F., Influence of slag chemistry on the hydration of alkali-activated blast-furnace slag – Part 1: Effect of MgO, Cement and Concrete Research, 41, 2011, pp 955-963

[69] BRINDLEY, G.W., and KIKKAWA, S., A crystal-chemical study of Mg,Al and Ni,N hydroxy-perchlorates and hydroxycarbonates. American Mineralogist, 1979. 64(7-8): p. p. 836 - 843.

[70] ROBLER, M., ODLER, I., Investigation on the Relationship Between Porosity, Structure and Strength of Hydrated Portland Cement Pastes I – Effect of Porosity, Cement and Concrete Research, 15, 1985, pp. 320-330

[71] IGARASHI, S., KAWAMURA, M, WATANABE, A., Analysis of cement pastes and mortars by a combination of backscatter-based SEM image analysis and calculations based on the Powers model, Cement and Concrete Composites, 26, 2004, pp. 977–985.

[72] ZAJAC, M., BEN HAHA, M., Experimental investigation and modeling of hydration and performance evolution of fly ash cement, Materials and Structures, 47, 2013, pp, 1259-1269

[73] TERMKHAJORNKIT, P., VU, Q.H., BARBARULO, R., DARONNAT, S., CHANVILLARD, G., Dependence of Compressive Strength on Phase Assemblage in Cement Pastes: Beyond Gel-Space Ratio – Experimental Evidence and Micromechanical Modelling, Cement and Concrete Research, 56, 2014, pp. 1-11

[74] BENTUR, A., Effect of Gypsum on the Hydration and Strength of C_3S pastes, Journal of American Ceramic Society, 59, 1976, pp. 210-213

[75] JELENIC, I., PANOVIC, A., HALLE, R., GACESA, T., Effect of Gypsum on the Hydration and Strength Development of Commercial Portland Cements Containing Alkali Sulfates, Cement and Concrete Research, 7, 1977, pp. 239-246

[76] GUNAY, S., GARRAULT. S., NONAT, A., TERMKHAJORNKIT, P., Influence of Calcium Sulphate on Hydration and Mechanical Strength of Tricalcium silicate, Proceedings of the 13th ICCC, Madrid, Spain, 2011

[77] MEDALA, M., Etudes des Interactions entre les phases minérales constituant le ciment Portland et des solutions salinesées, PhD Thesis, Dijon, 2005

[78] SERSALE, R., CIOFFI, R., FRIGIONE, G., ZENONE, F., Relationship Between Gypsum Content, Porosity and Strength in Cement, Cement and Concrete Research, 21, 1991, 00. 120-126

Figure 1

Click here to download high resolution image

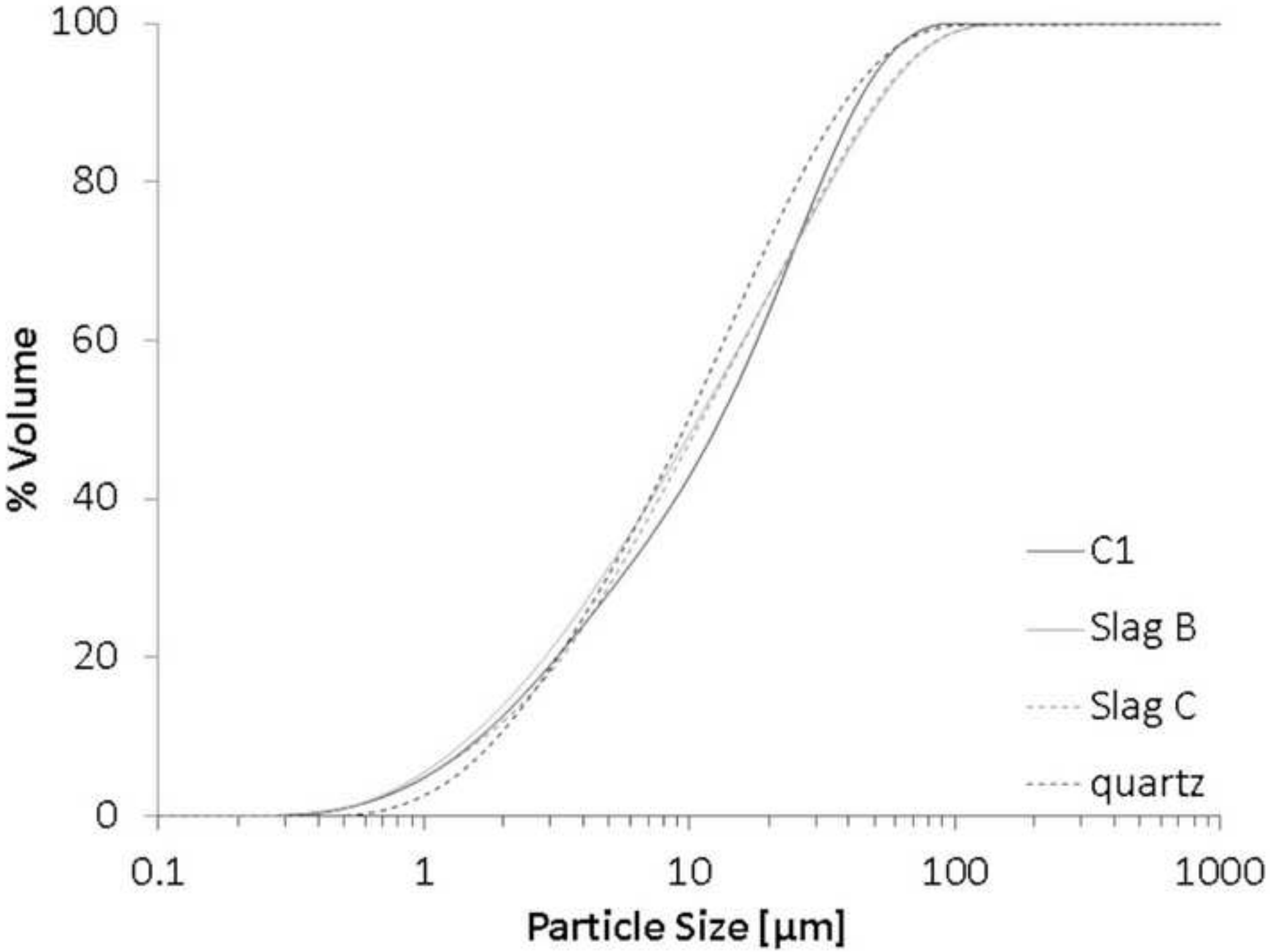

Figure 2a
Click here to download high resolution image

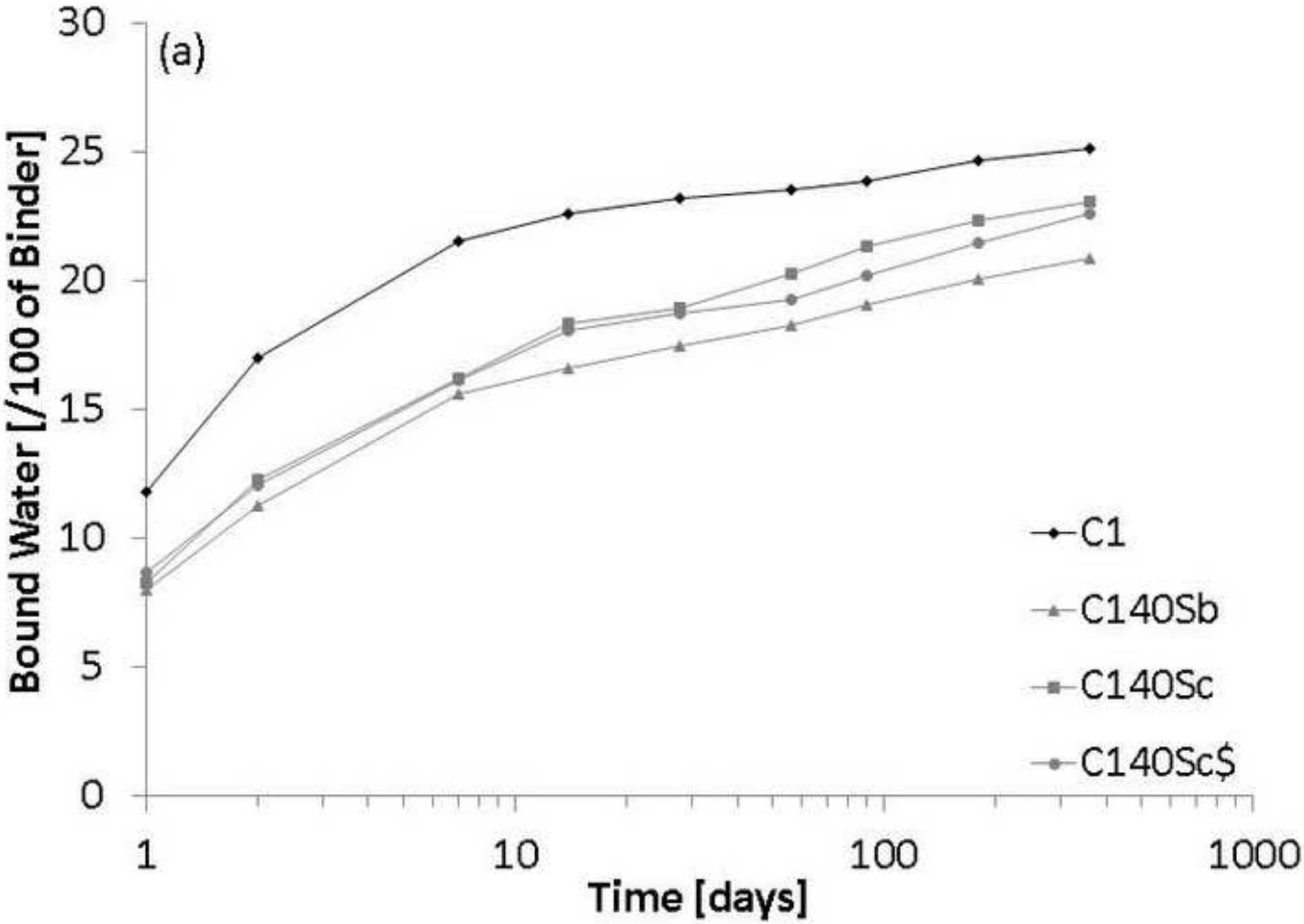

Figure 2b
Click here to download high resolution image

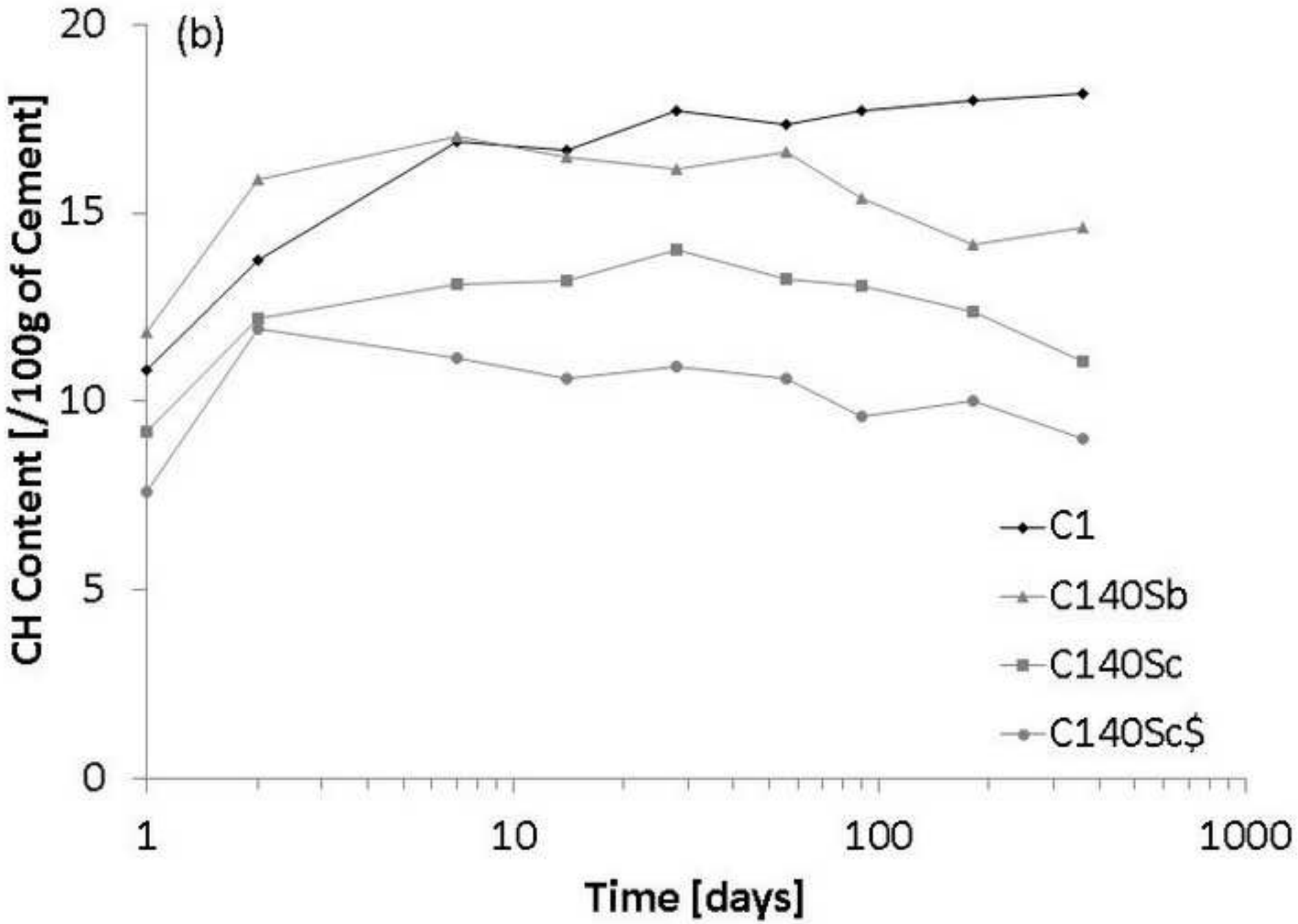

Figure 3a
Click here to download high resolution image

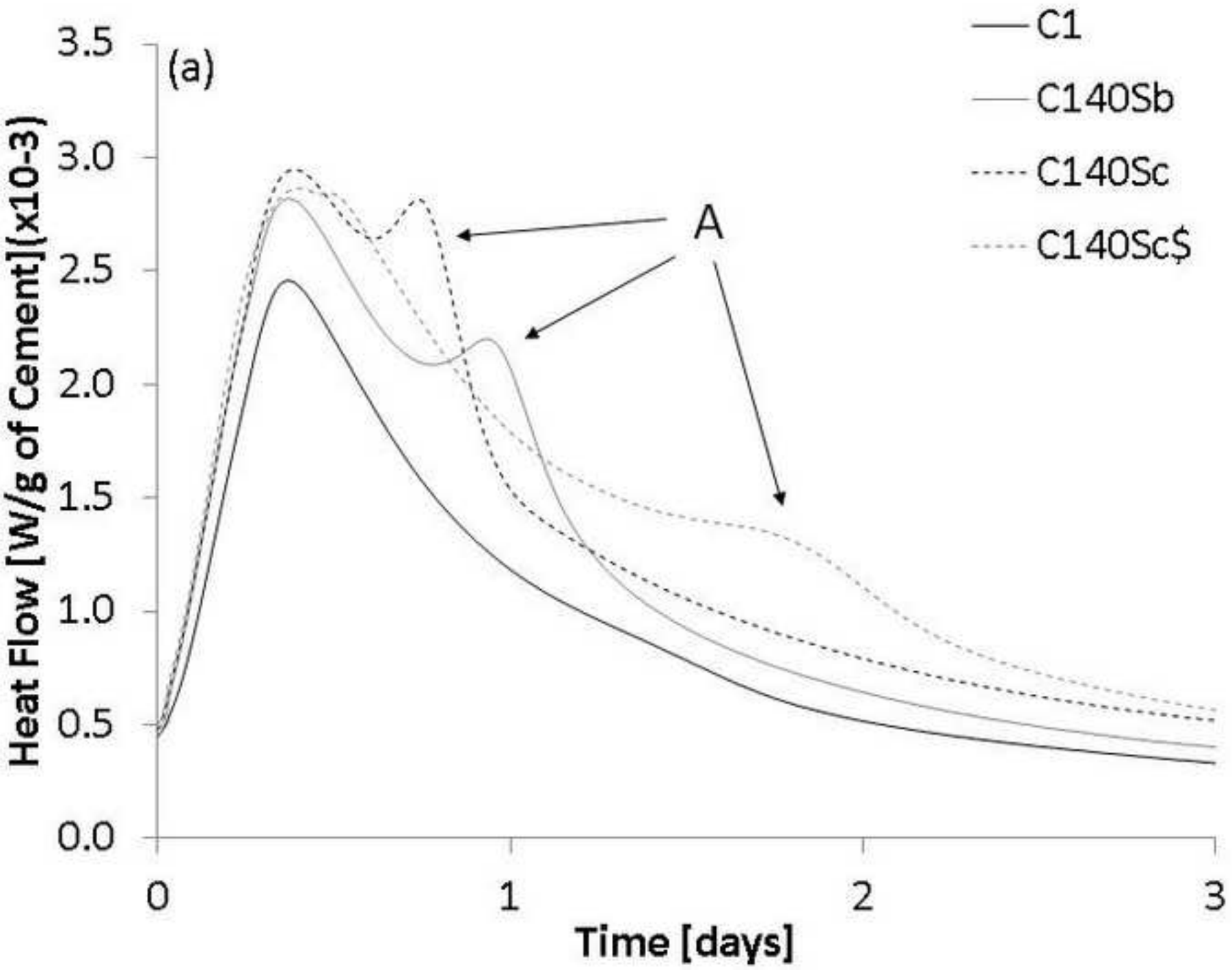

Figure 3b
Click here to download high resolution image

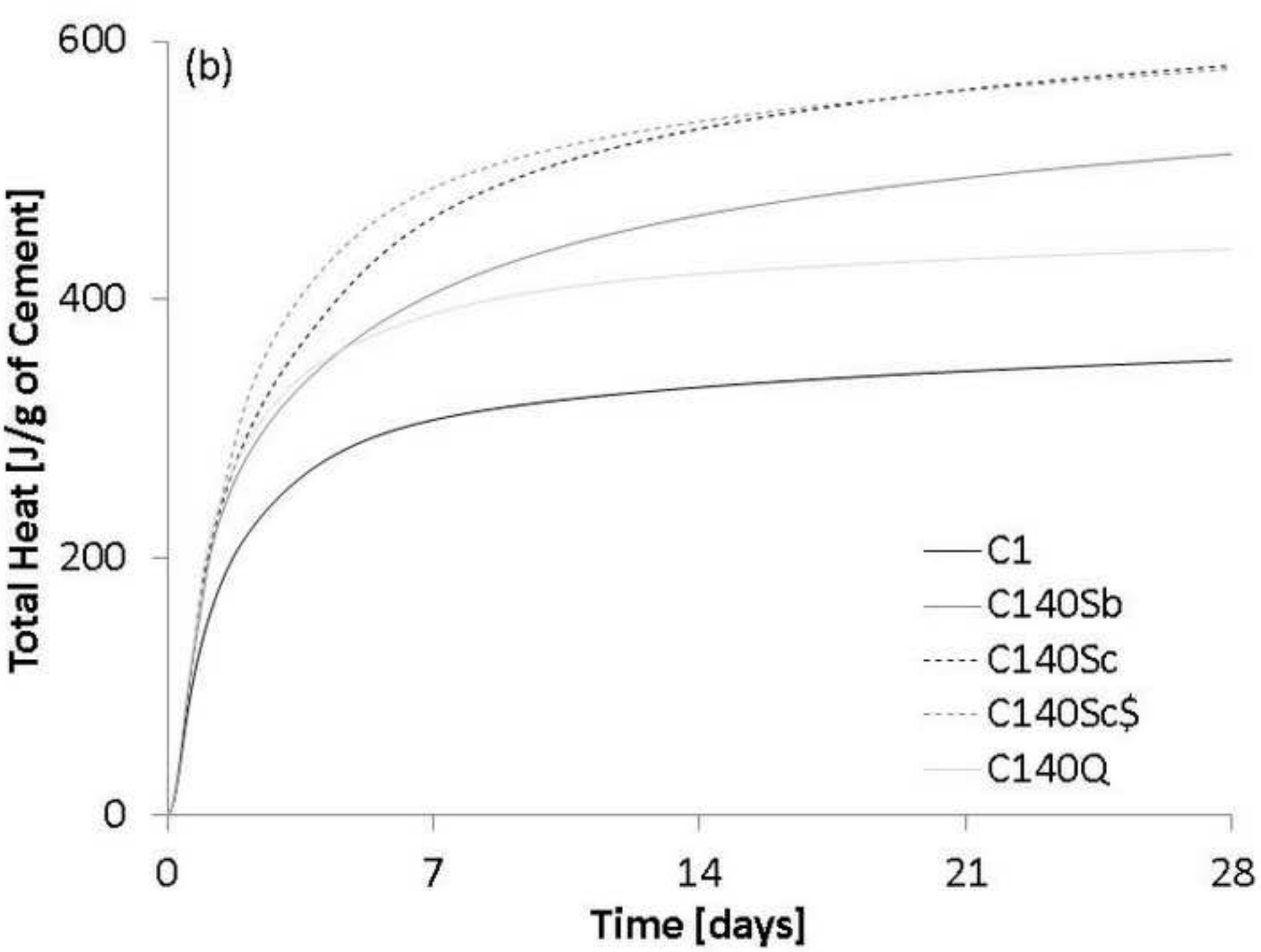

Figure 4
Click here to download high resolution image

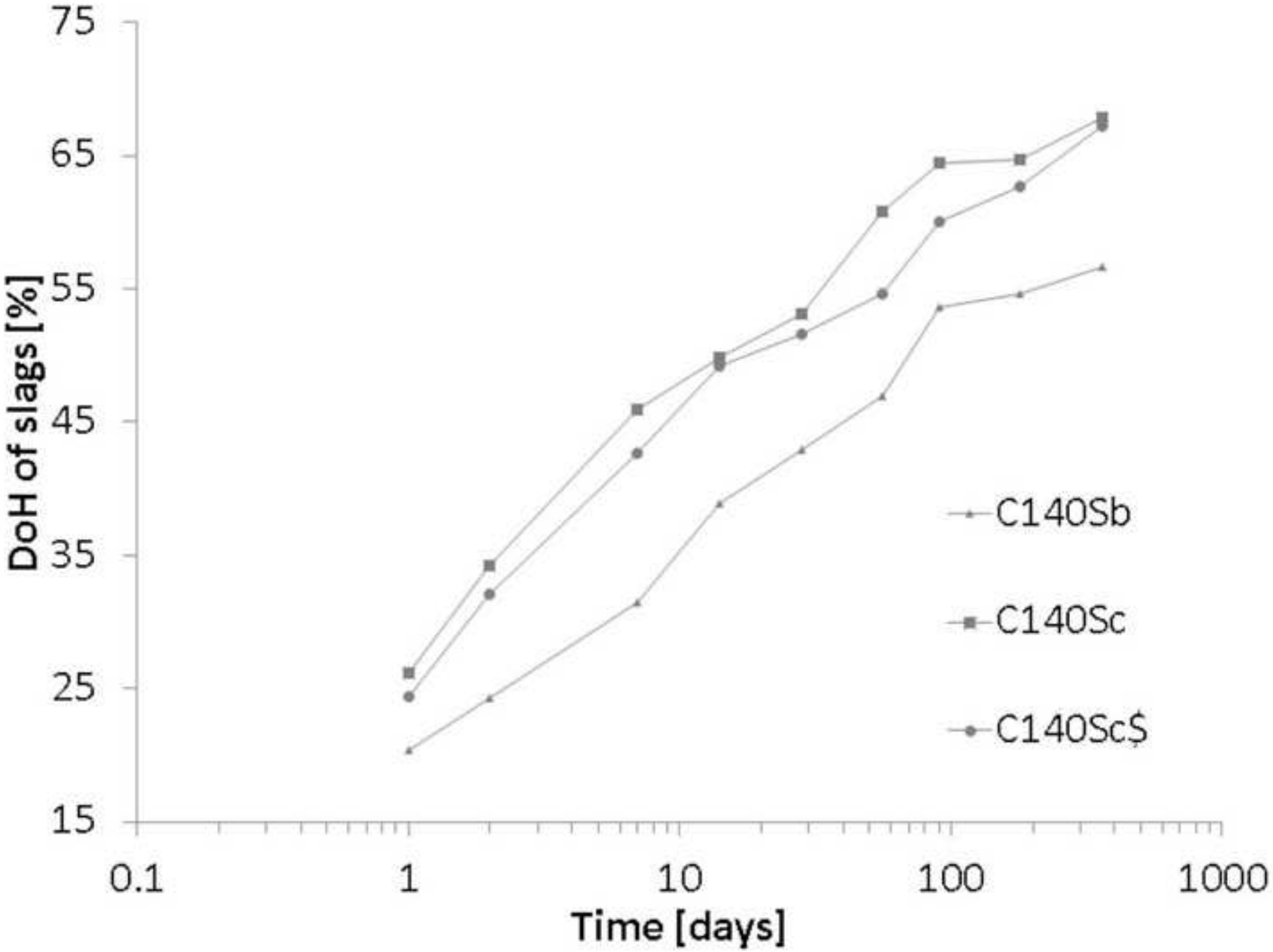

Figure 5
Click here to download high resolution image

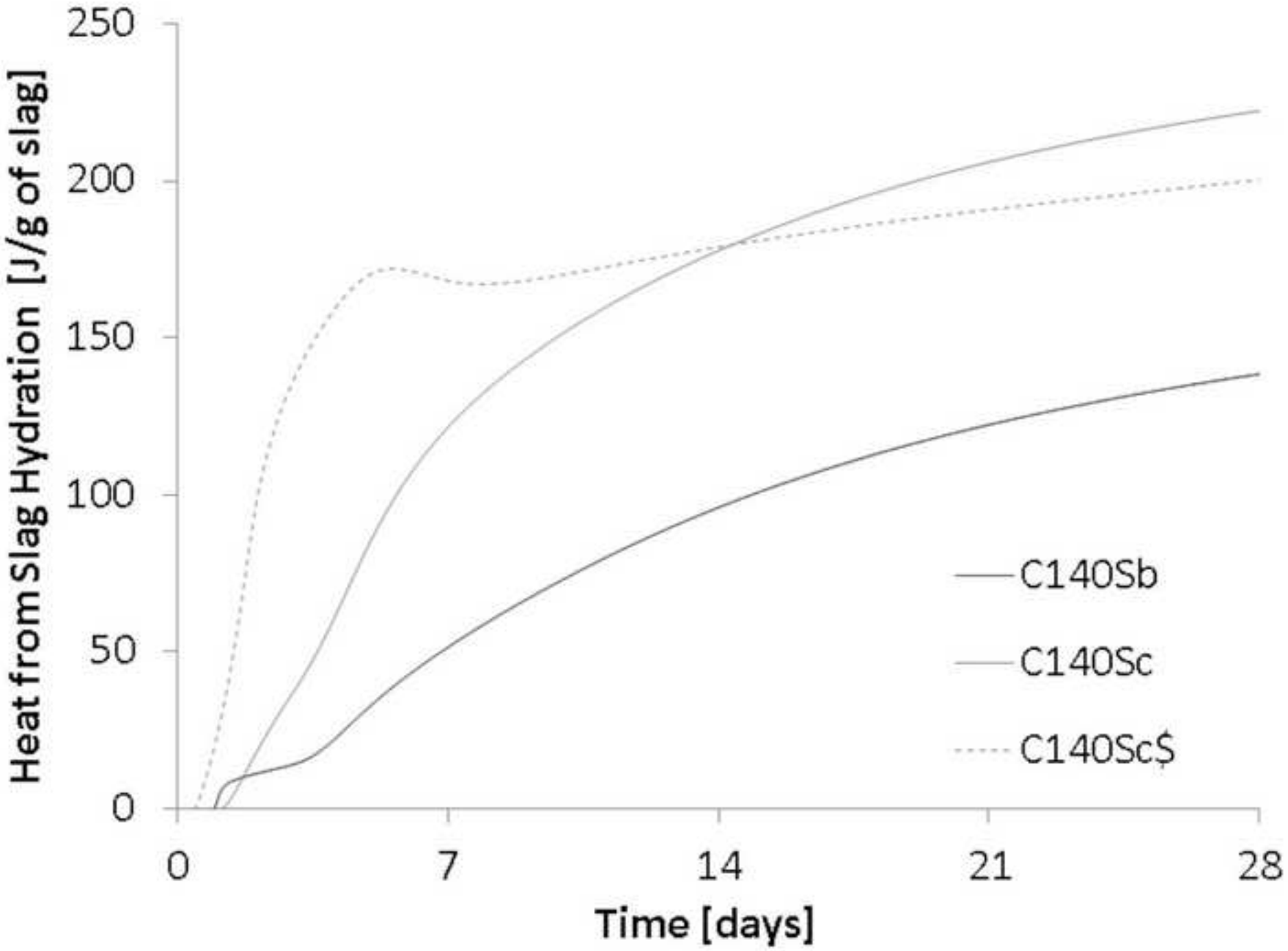

Figure 6

Click here to download high resolution image

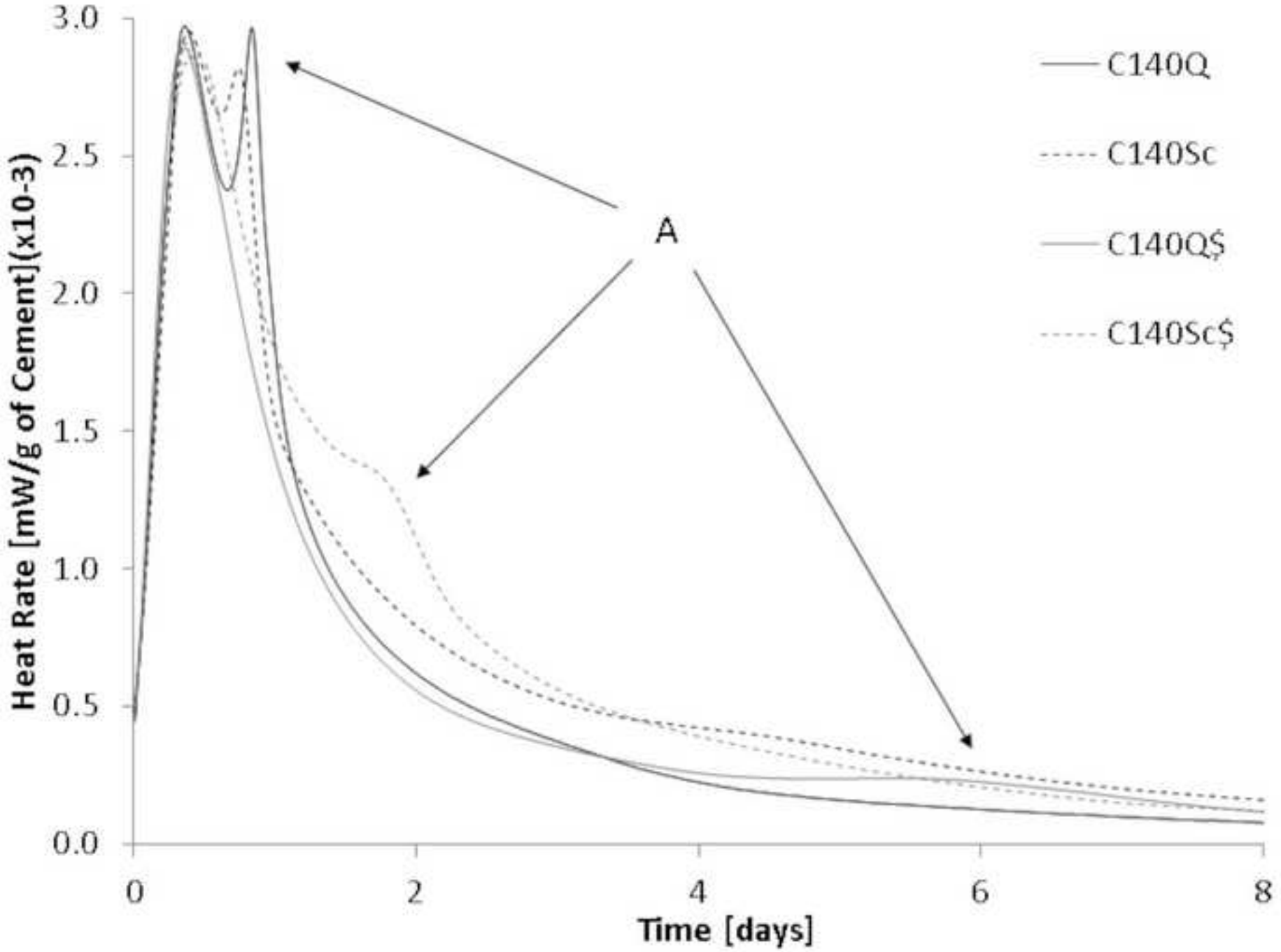

Figure 7

Click here to download high resolution image

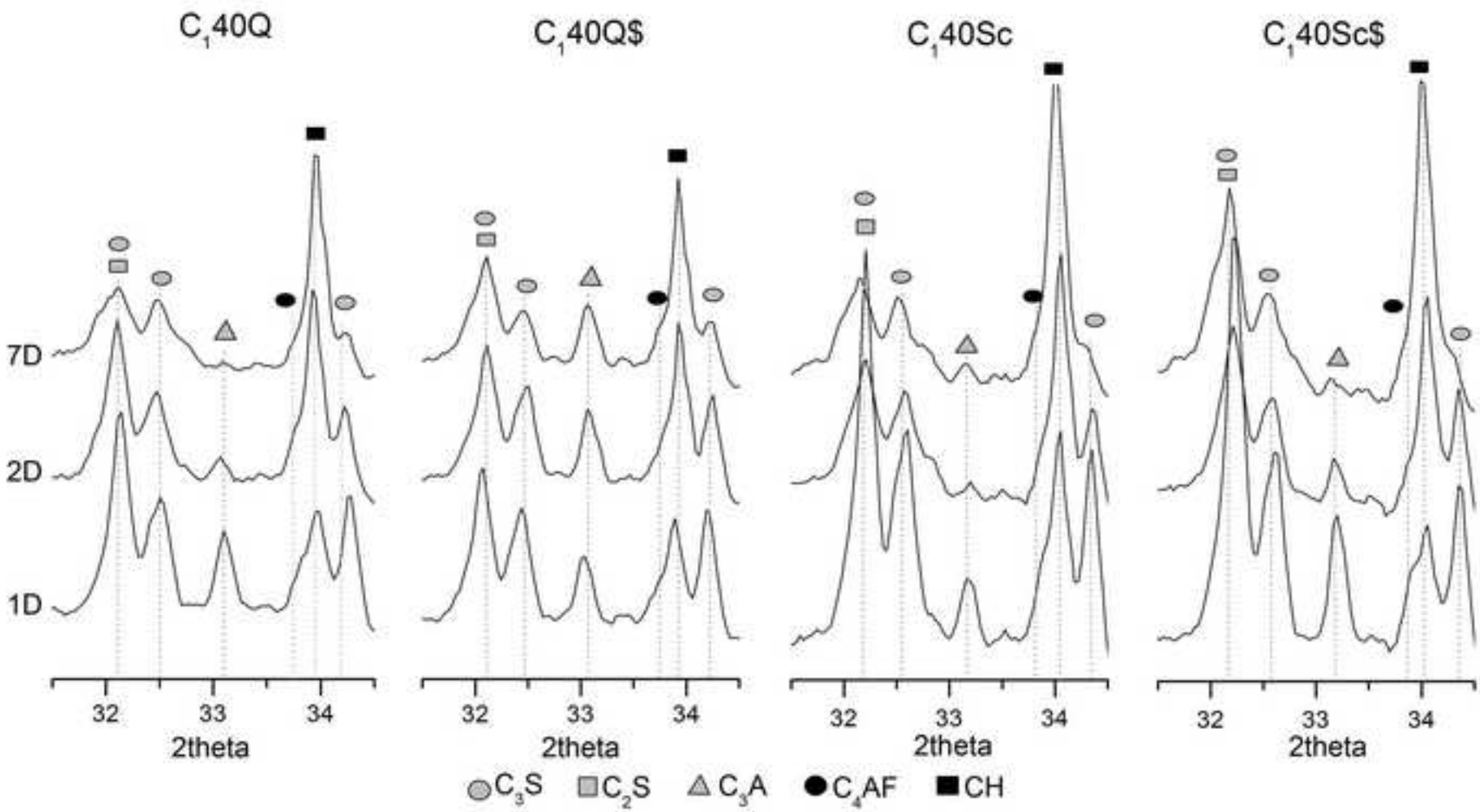

Figure 8a
Click here to download high resolution image

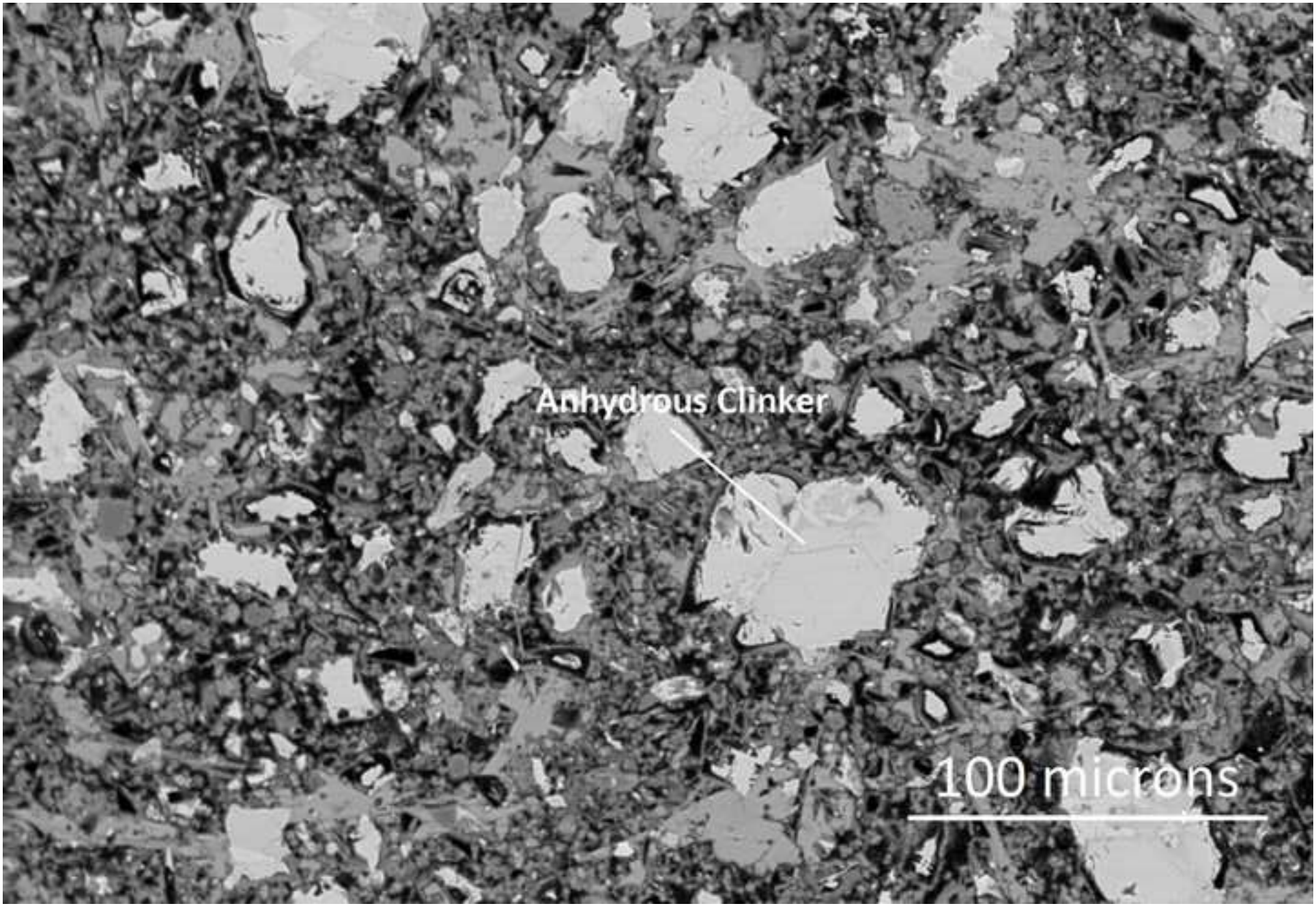

Figure 8b
Click here to download high resolution image

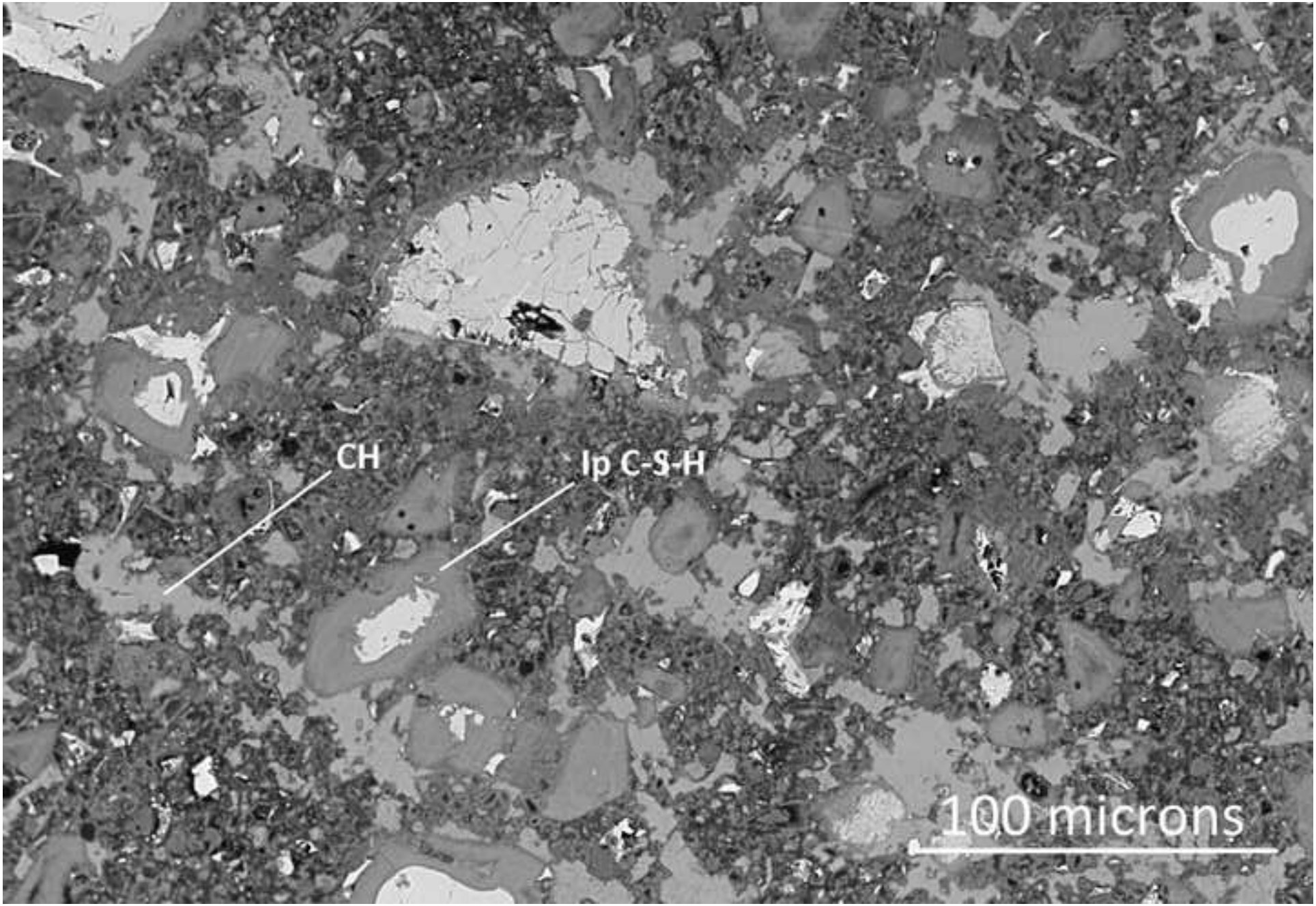

Figure 8c

Click here to download high resolution image

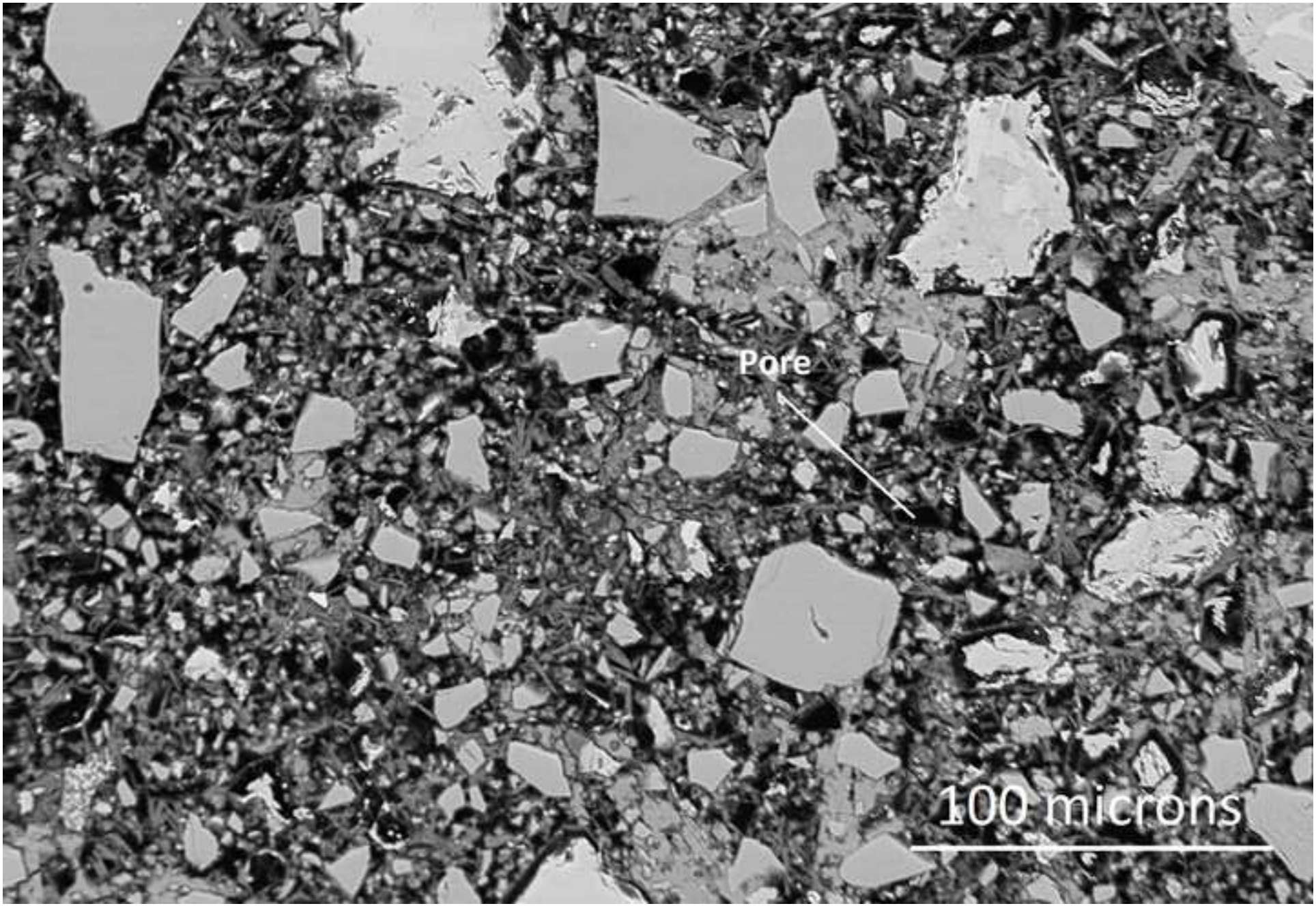

Figure 8d
Click here to download high resolution image

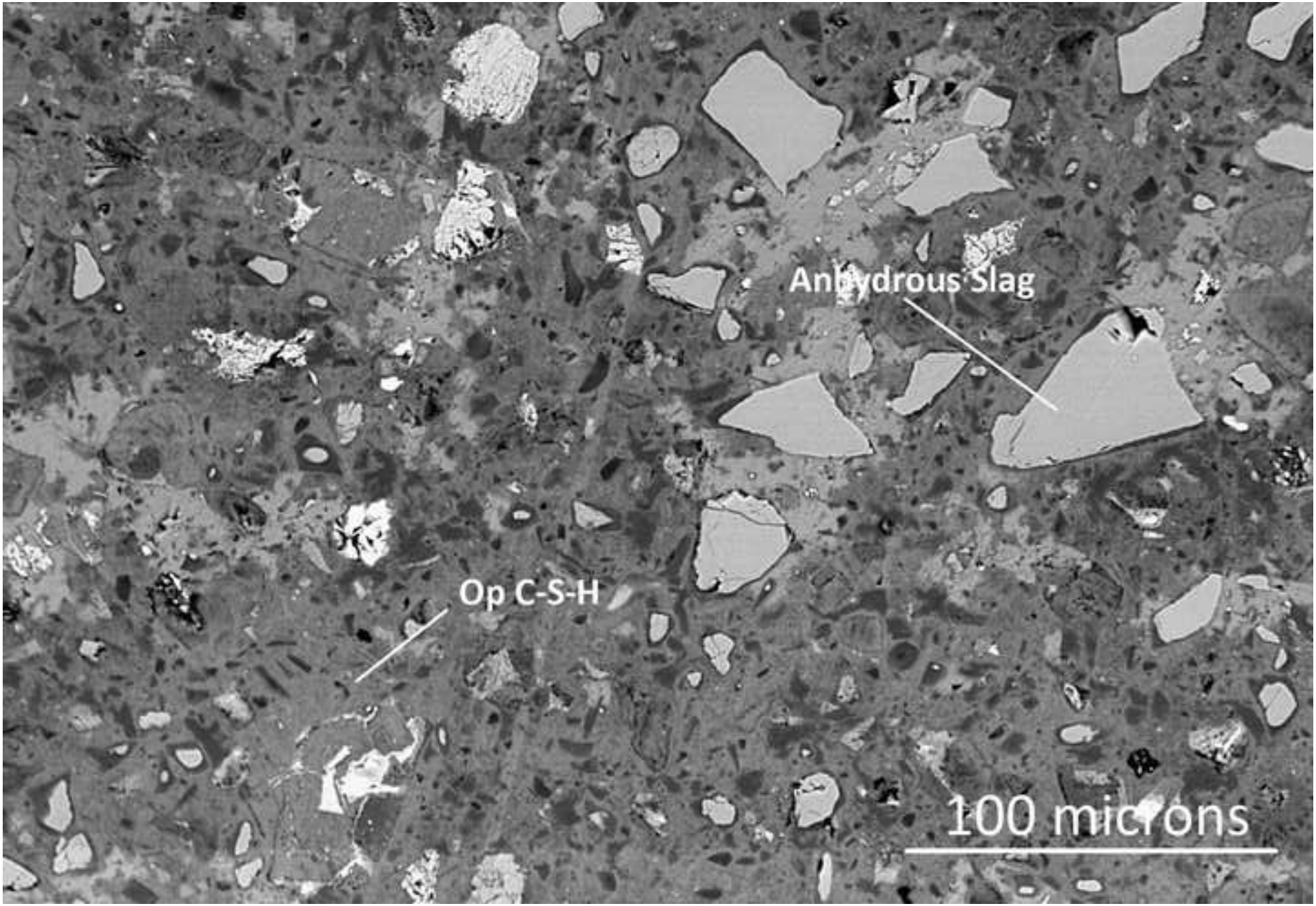

Figure 9

Click here to download high resolution image

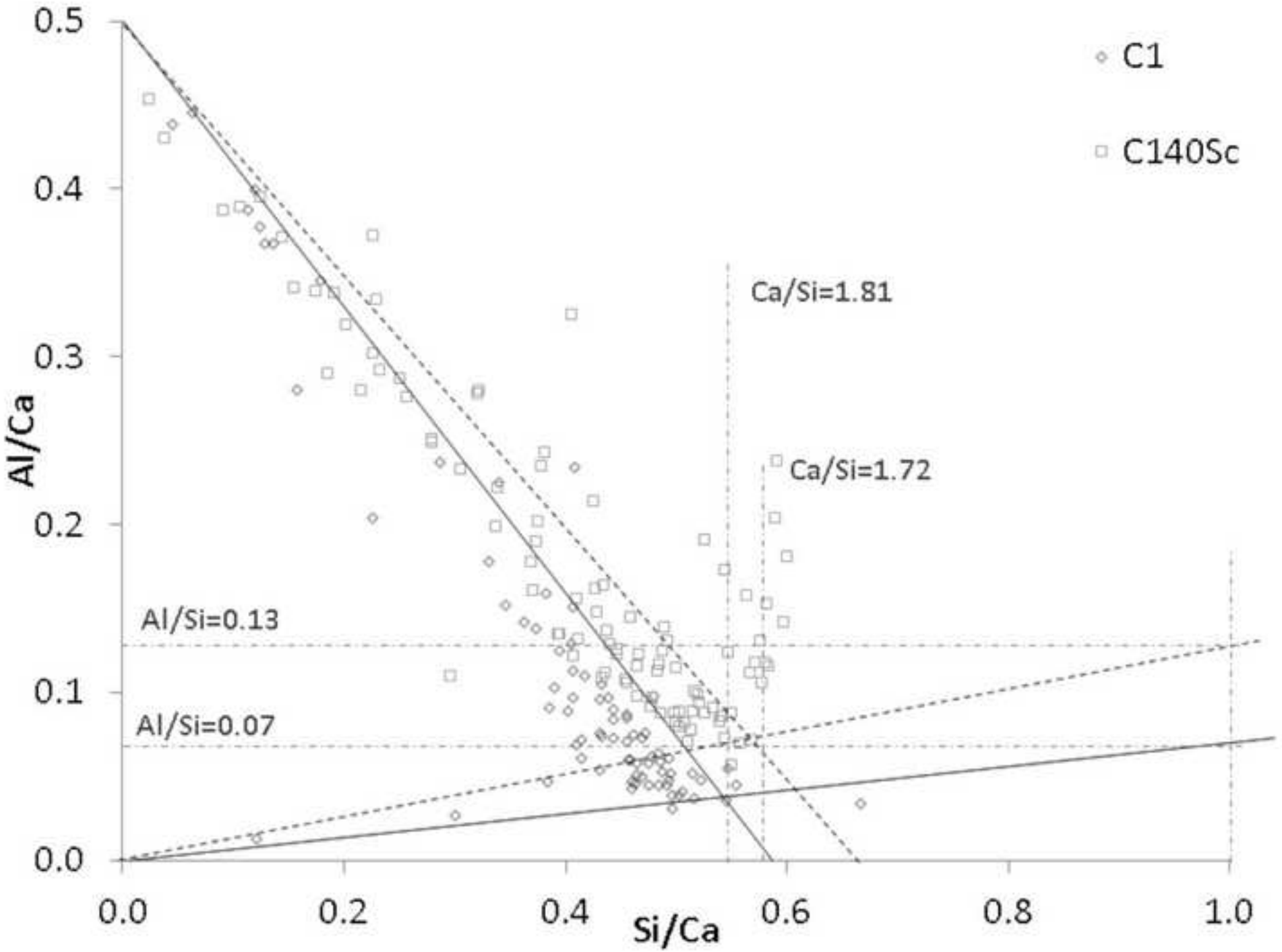

Figure 10
Click here to download high resolution image

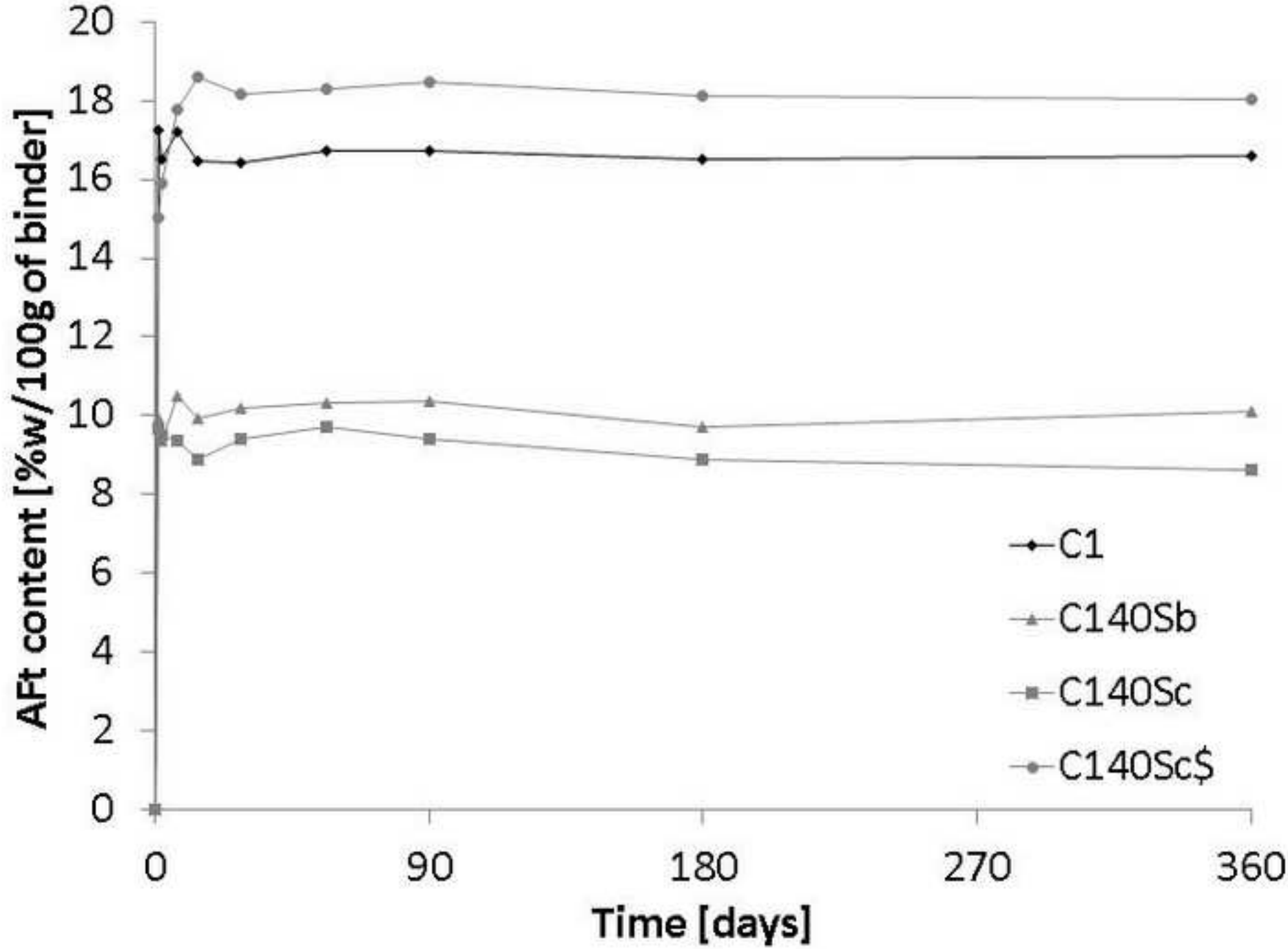

Figure 11

Click here to download high resolution image

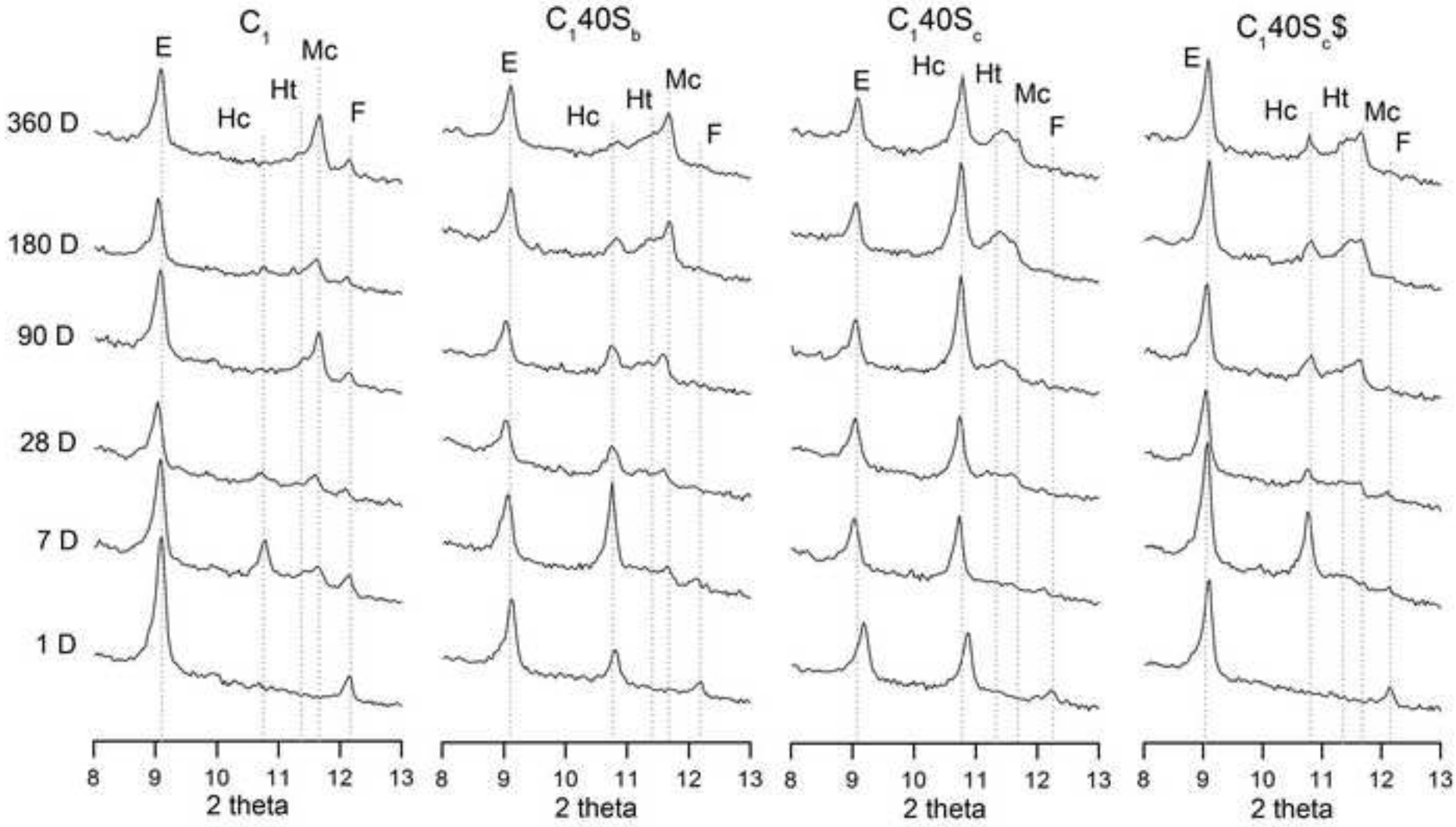

Figure 12

Click here to download high resolution image

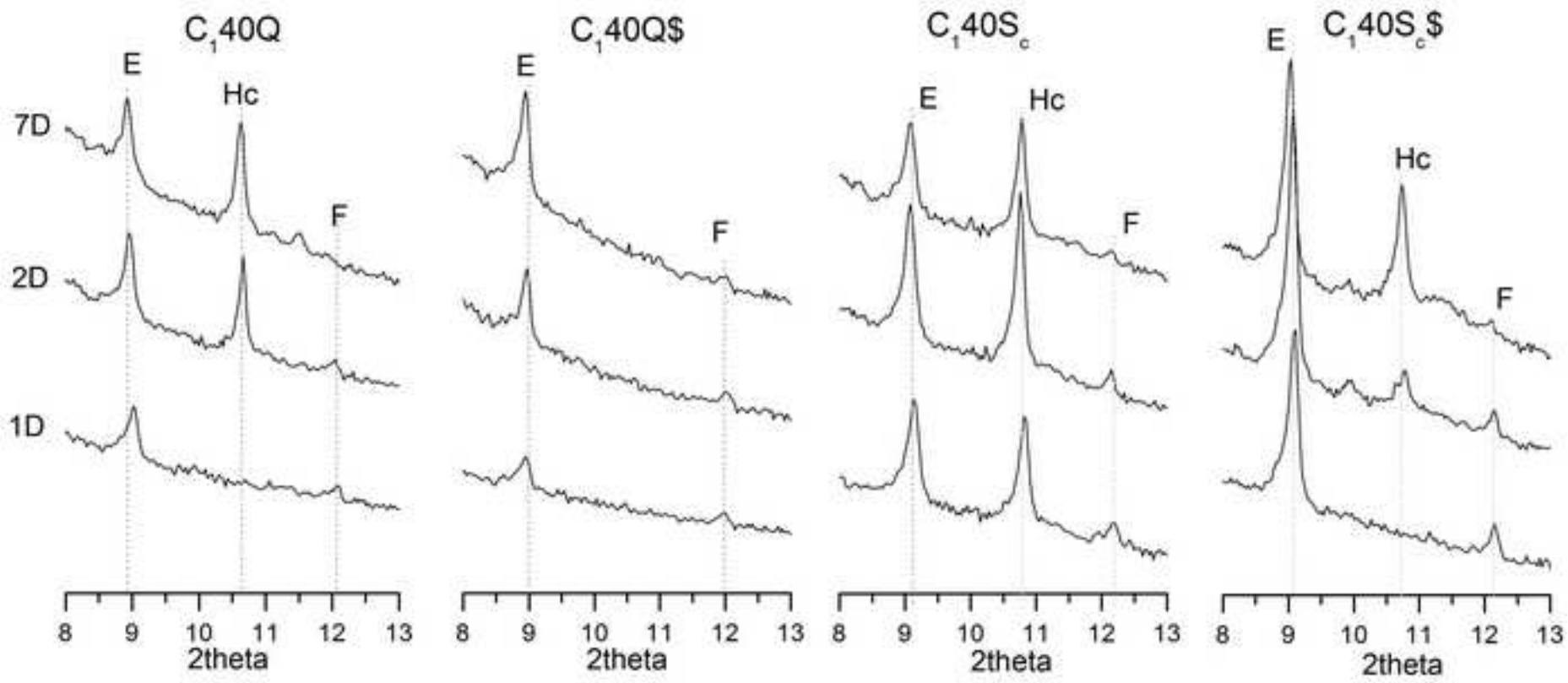

Figure 13

Click here to download high resolution image

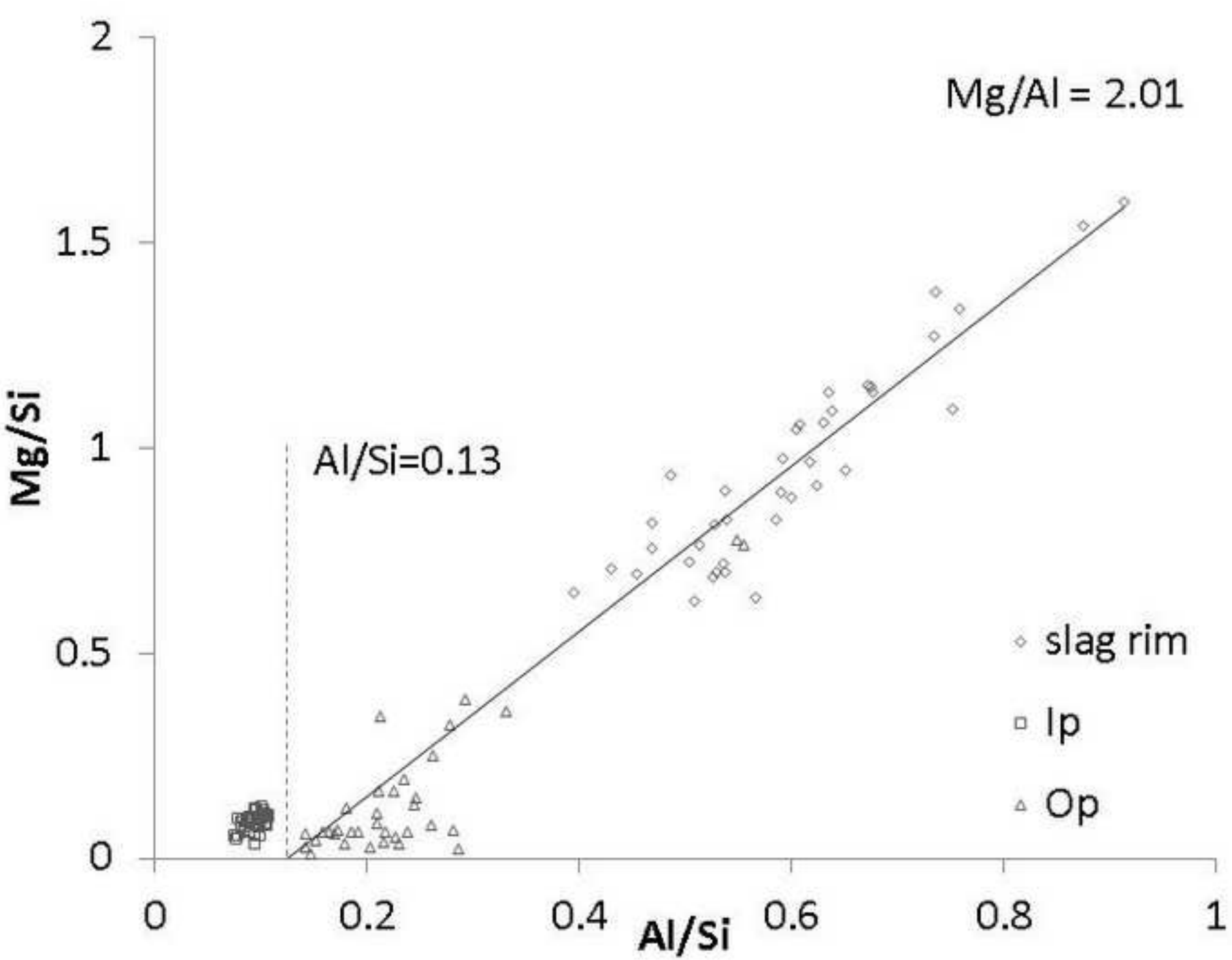

Figure 14
Click here to download high resolution image

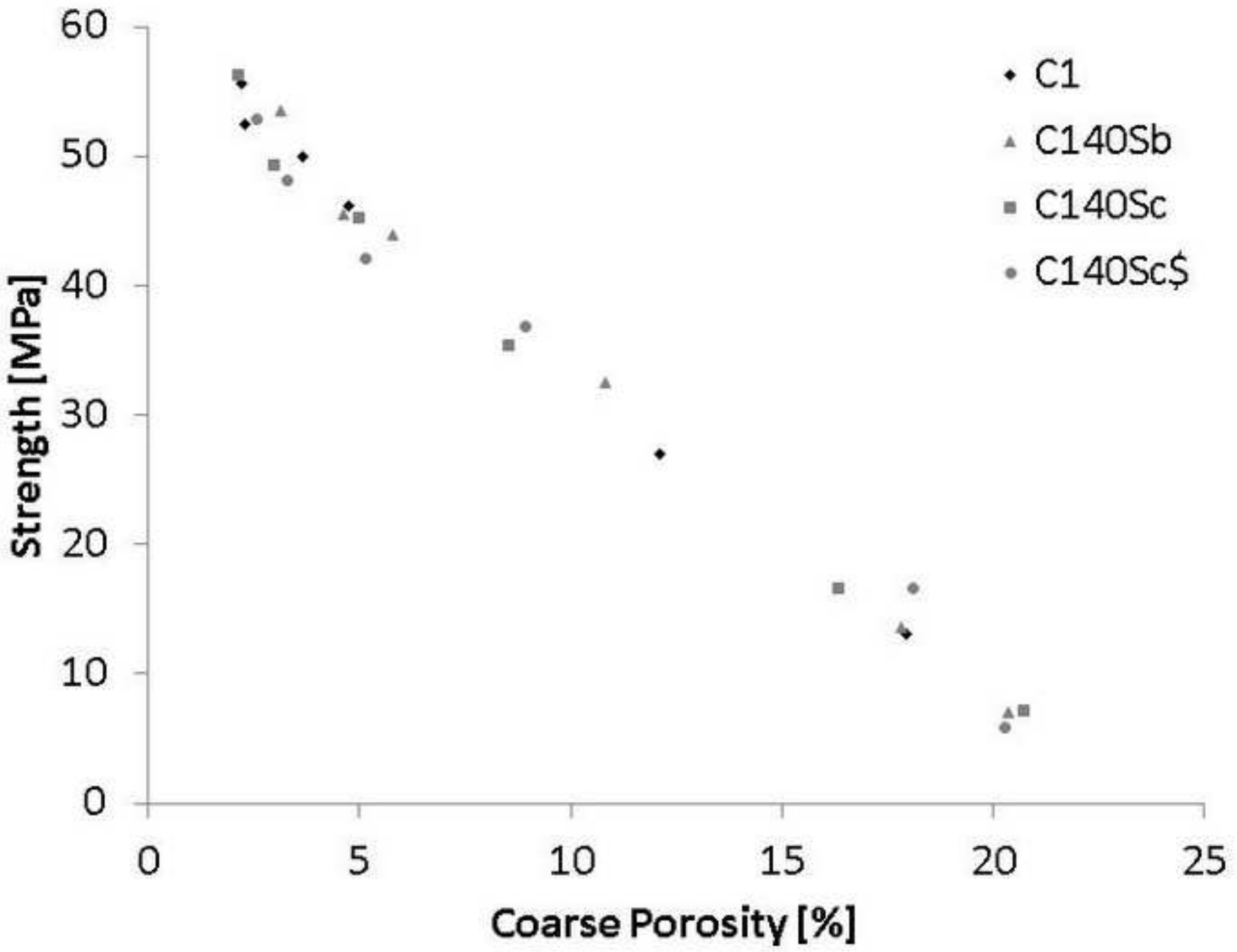

Figure 15

Click here to download high resolution image

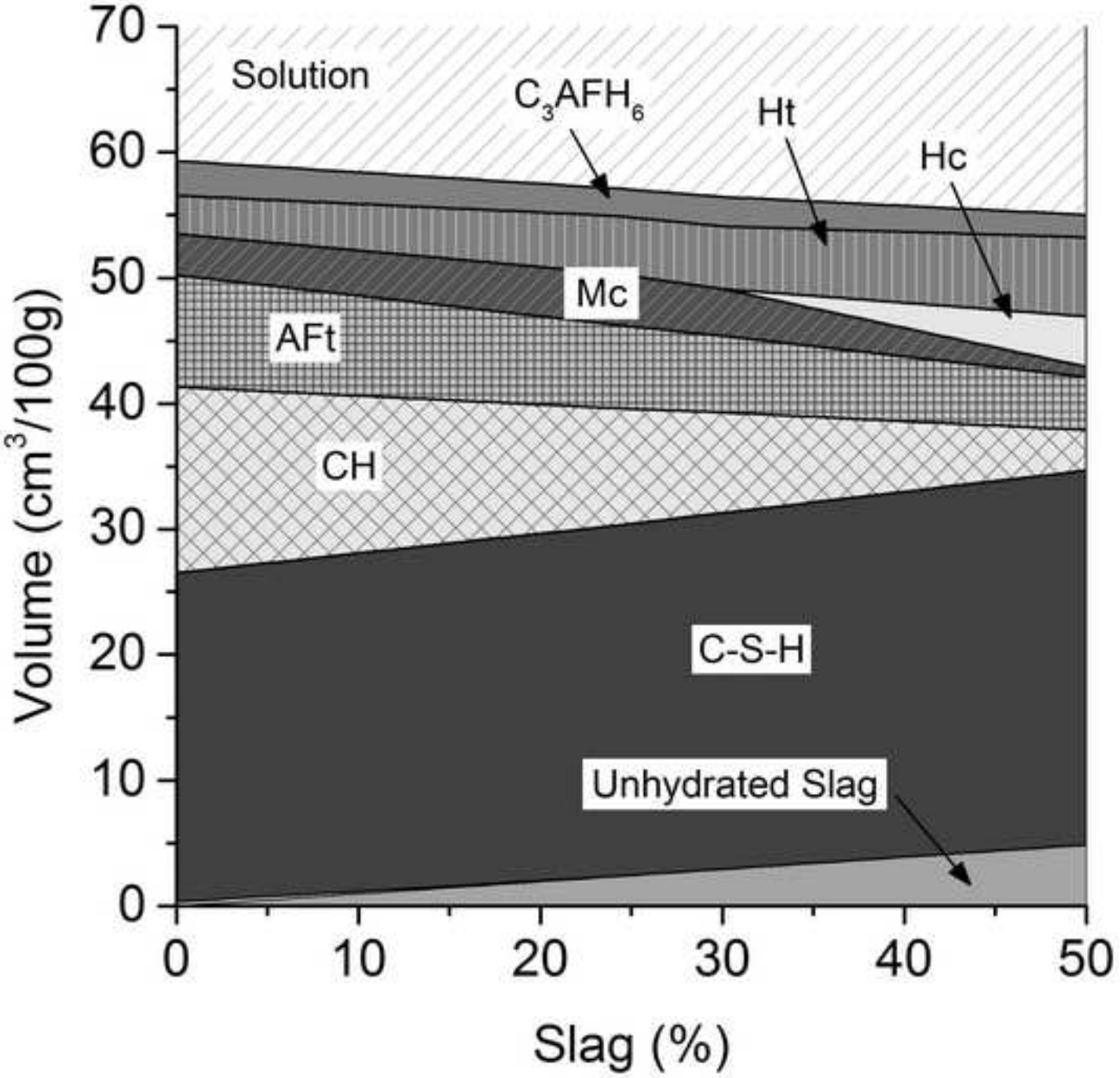

Figure 16
Click here to download high resolution image

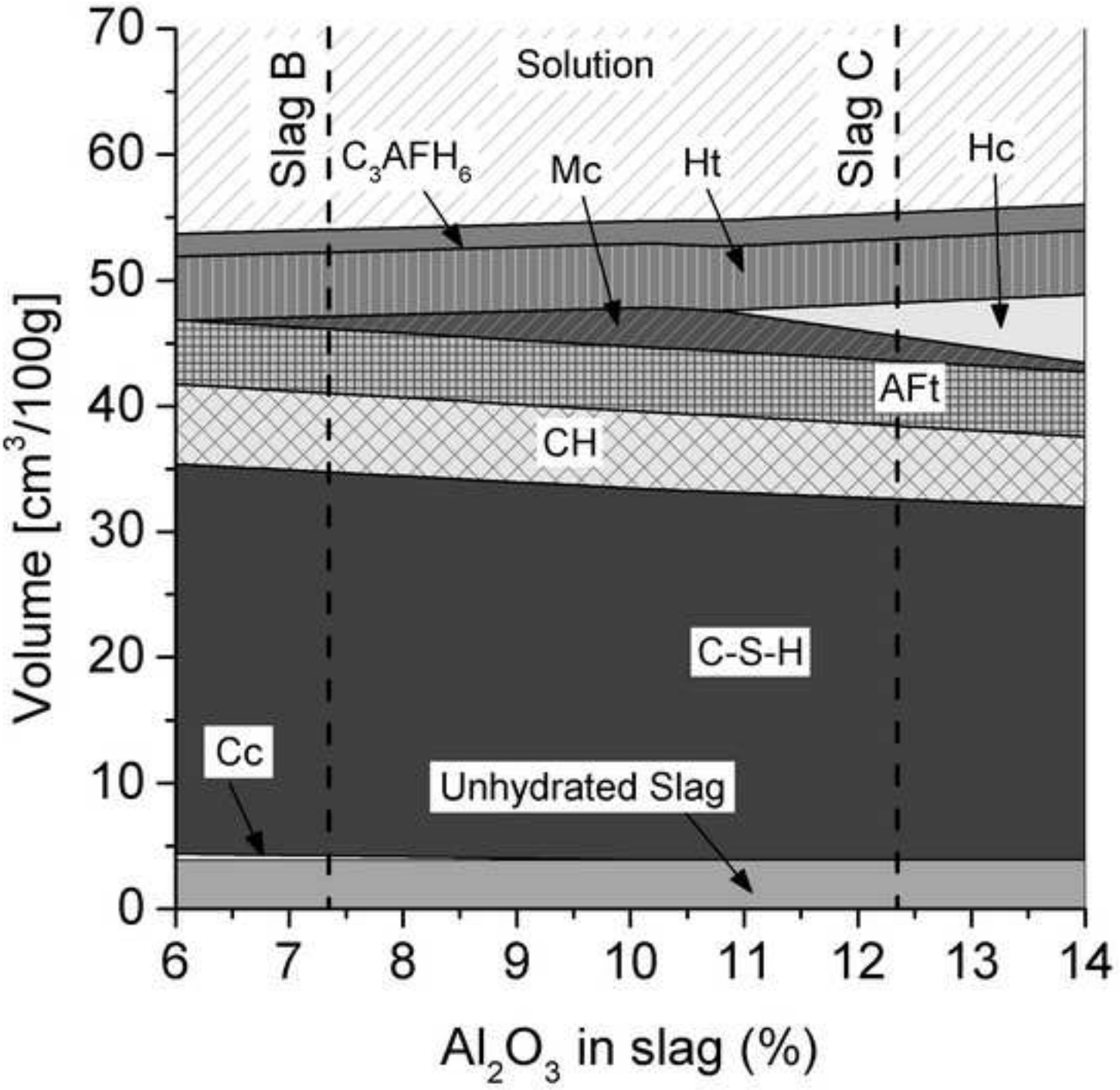

Figure 17
Click here to download high resolution image